JBC RESEARCH ARTICLE

Chemokine-like MDL proteins modulate flowering time and innate immunity in plants

Received for publication, January 22, 2021, and in revised form, March 18, 2021 Published, Papers in Press, March 30, 2021,
https://doi.org/10.1016/j.jbc.2021.100611

Katrin Gruner[1], Franz Leissing[1], Dzmitry Sinitski[2], Hannah Thieron[1], Christian Axstmann[1], Kira Baumgarten[1], Anja Reinstädler[1], Pascal Winkler[1], Melina Altmann[3], Andrew Flatley[4], Maëlle Jaouannet[5], Krzysztof Zienkiewicz[6,7], Ivo Feussner[6,7], Harald Keller[5], Christine Coustau[5], Pascal Falter-Braun[3,8], Regina Feederle[4,9], Jürgen Bernhagen[2,9,*], and Ralph Panstruga[1,*]

From the [1]RWTH Aachen University, Institute for Biology I, Unit of Plant Molecular Cell Biology, Aachen, Germany; [2]Ludwig-Maximilians-University (LMU), LMU University Hospital, Chair of Vascular Biology, Institute for Stroke and Dementia Research (ISD), Munich, Germany; [3]Helmholtz Center Munich, German Research Center for Environmental Health, Institute of Network Biology (INET), Munich-Neuherberg, Germany; [4]Helmholtz Center Munich, German Research Center for Environmental Health, Institute for Diabetes and Obesity, Monoclonal Antibody Core Facility, Munich-Neuherberg, Germany; [5]Institut Sophia Agrobiotech, Université Côte d'Azur, INRAE, CNRS, Sophia Antipolis, France; [6]University of Goettingen, Albrecht von Haller Institute and Goettingen Center for Molecular Biosciences (GZMB), Department of Plant Biochemistry, Goettingen, Germany; [7]University of Goettingen, Goettingen Center for Molecular Biosciences (GZMB), Service Unit for Metabolomics and Lipidomics, Goettingen, Germany; [8]Ludwig-Maximilians-Universität (LMU), Faculty of Biology, Chair of Microbe-Host Interactions, Planegg-Martinsried, Germany; and [9]Munich Cluster for Systems Neurology (SyNergy), Munich, Germany

Edited by Joseph Jez

Human macrophage migration inhibitory factor (MIF) is an atypical chemokine implicated in intercellular signaling and innate immunity. MIF orthologs (MIF/D-DT-like proteins, MDLs) are present throughout the plant kingdom, but remain experimentally unexplored in these organisms. Here, we provide an *in planta* characterization and functional analysis of the three-member gene/protein MDL family in *Arabidopsis thaliana*. Subcellular localization experiments indicated a nucleo-cytoplasmic distribution of MDL1 and MDL2, while MDL3 is localized to peroxisomes. Protein–protein interaction assays revealed the *in vivo* formation of MDL1, MDL2, and MDL3 homo-oligomers, as well as the formation of MDL1-MDL2 hetero-oligomers. Functionally, *Arabidopsis mdl* mutants exhibited a delayed transition from vegetative to reproductive growth (flowering) under long-day conditions, but not in a short-day environment. In addition, *mdl* mutants were more resistant to colonization by the bacterial pathogen *Pseudomonas syringae* pv. *maculicola*. The latter phenotype was compromised by the additional mutation of *SALICYLIC ACID INDUCTION DEFICIENT* 2 (*SID2*), a gene implicated in the defense-induced biosynthesis of the key signaling molecule salicylic acid. However, the enhanced antibacterial immunity was not associated with any constitutive or pathogen-induced alterations in the levels of characteristic phytohormones or defense-associated metabolites. Interestingly, bacterial infection triggered relocalization and accumulation of MDL1 and MDL2 at the peripheral lobes of leaf epidermal cells. Collectively, our data indicate redundant functionality and a complex interplay between the three chemokine-like *Arabidopsis* MDL proteins in the regulation of both developmental and immune-related processes. These insights expand the comparative cross-kingdom analysis of MIF/MDL signaling in human and plant systems.

Human macrophage migration inhibitory factor (MIF) is a small (114 amino acids, 12.345 kDa) multifunctional protein that is best known for its role as an atypical cytokine/chemokine to regulate innate immunity. In fact, MIF was the first human cytokine to be discovered over five decades ago (1–3). Dysregulation of MIF has been associated with acute and chronic inflammatory diseases such as septic shock, rheumatoid arthritis, and atherosclerosis, as well as autoimmune conditions and cancer (4–7). The expression of MIF in the human organism is not limited to immune cells but is broadly detectable in various tissues and cell types. Unlike other cytokines/chemokines, MIF lacks a canonical N-terminal signal peptide and is released from preformed intracellular stores into the extracellular environment *via* stimulus-regulated unconventional secretion (1, 8). MIF's cytokine/chemokine activities are mediated through interaction with its cognate receptor CD74 and/or by noncognate engagement of one of its three CXC chemokine receptors in a cell-, tissue-, or disease-specific manner (1, 3, 9, 10). CD74 is a single-pass transmembrane protein, also known as the human HLA class II histocompatibility antigen γ chain (9, 11). Upon MIF binding, signaling from cell-surface-expressed CD74 prominently regulates cell proliferation, apoptosis, and inflammatory gene expression. The chemokine receptors of MIF, CXCR2, CXCR4, and CXCR7, belonging to the class of heptahelical membrane proteins, function as G-protein-coupled receptors (GPCRs) and are the *bona fide* receptors for classical chemokines such as CXCL8, CXCL12, and CXCL11, respectively. MIF engages

* For correspondence: Ralph Panstruga, panstruga@bio1.rwth-aachen.de; Jürgen Bernhagen, Juergen.Bernhagen@med.uni-muenchen.de.

these receptors *via* a structural mimicry mechanism to promote leukocyte recruitment responses that can play an important pathogenic role in cardiovascular and inflammatory diseases (6, 7, 10).

In addition to its cytokine/chemokine functions in the extracellular space ("MIF the cytokine"), MIF has a number of suggested intracellular functions mediated by protein–protein interactions or enzymatic activity. This is in line with its high degree of evolutionary conservation, and it has been speculated that intracellular, enzymatic activities of MIF are evolutionarily ancient ("MIF the enzyme") (3). Reported enzymatic activities comprise a tautomerase activity linked to an N-terminal proline-containing catalytic pocket (3, 12), an oxidoreductase activity that is dependent on a central CXXC motif (3, 13), a nuclear endonuclease activity (3, 14), as well as a chaperone-like role (3, 15). However, the precise molecular mechanisms of these activities and their potential interplay are incompletely understood and their physiological significance remains elusive. Many vertebrates including humans possess a paralog of MIF, termed D-dopachrome tautomerase (D-DT) or MIF-2. In humans, D-DT/MIF-2 shares approximately 35% amino acid identity and a high degree of architectural similarity with MIF, and the protein recapitulates some of MIF's pathogenic activities. However, the physiological and pathogenic functions of D-DT are less well characterized than those of MIF (16, 17).

MIF-like proteins are conserved in most eukaryotes, including plants, with signs of neofunctionalization in some taxa (18, 19). Previously, we performed a comprehensive *in silico* analysis of plant MIF/D-DT-like (MDL) proteins, focusing on the dicotyledonous reference plant species *Arabidopsis thaliana* (20). We found that seed plants typically express two (gymnosperms) or three (angiosperms) different paralogs, which in *Arabidopsis* have been named MDL1 (AT5G57170), MDL2 (AT5G01650), and MDL3 (AT3G51660). Publicly accessible microarray data indicate that *MDL1* and *MDL2* are essentially expressed constitutively in aerial plant organs with little responsiveness to abiotic or biotic stress cues, while expression of *MDL3* appears to be stress-inducible. The latter gene exhibits strongly enhanced transcript accumulation in leaves upon various abiotic (cold treatment, osmotic and oxidative stress, wounding, UV-B exposure) and biotic (microbial elicitors, various pathogens) stress factors. *MDL3* shows in addition coexpression with a number of prominent genes involved in plant immunity (20). Structure prediction and preliminary experimental data suggest that all three *Arabidopsis* MDL proteins resemble the secondary and tertiary structure of human MIF (20, 21).

In contrast to human and murine MIF, very little is known about the function of plant MDLs. Analysis of recombinant epitope-tagged *Arabidopsis* MDLs revealed an unexpected lack of tautomerase activity, which is possibly conditioned by an amino acid polymorphism in their catalytic clefts. Surprisingly, the three MDLs can bind to the human MIF receptors CD74 and CXCR4 (which are absent from plants), activate signaling activities downstream of these in human immune cells, and substitute for human MIF in leukocyte recruitment. These findings disclose cross-kingdom mimicry of human MIF by these plant orthologs and reflect their (partial) functional conservation (21, 22). Reminiscent of the situation of human immune cells and some parasitic pathogens (19, 23), plant-feeding aphids secrete an MIF ortholog into host cells to suppress plant immune responses, which is necessary for their survival and nourishment (24).

Here, we functionally characterized the three *Arabidopsis* MDL proteins *in planta* by a comprehensive set of biochemical, cell biological, and genetic experiments. We validated the respective gene models, determined subcellular protein localizations, and studied their interactions, revealing the formation of MDL homo- and, in part, hetero-oligomers. Using a set of *mdl* mutants, we further uncovered roles for MDLs in the control of flowering time and bacterial pathogenesis.

Results

Arabidopsis MDL1 *and* MDL2 *are subject to alternative splicing*

The TAIR (The Arabidopsis Information Resource; https://www.arabidopsis.org/) database catalogs two different gene models for *MDL1* (designated *MDL1.1* and *MDL1.2*), four different gene models for *MDL2* (*MDL2.1*, *MDL2.2*, *MDL2.3*, and *MDL2.4*, leading to three different predicted protein variants), and a single gene model for *MDL3* (Fig. S1*A*, (20)). Protein structure prediction suggests that these transcript variants give rise to MDL forms with different C-terminal tail regions (Fig. S1*B*). To confirm experimentally the existence of the respective *MDL* transcript versions and to explore a putative tissue specificity of their expression, we first developed sets of splice variant-specific oligonucleotide primer pairs for reverse transcriptase–polymerase chain reaction (RT-PCR) (Fig. S1*C*). We validated the specificity of these primer pairs by using plasmid DNA harboring cloned versions of the various predicted *MDL* transcripts (except *MDL2.4*) as a template (Fig. S1*D*). Semiquantitative RT-PCR analysis of RNA samples from various *Arabidopsis* organs indicates that (i) all five tested *MDL1* and *MDL2* transcript variants exist (the used primer pairs did not discriminate between *MDL2.2* and *MDL2.3*; Fig. S1*C*), (ii) *MDL1.1* and *MDL2.1* appear to be the predominant transcript versions, and (iii) that there is no pronounced organ specificity in the accumulation of any of the various splice variants (Fig. S1*E*).

Subcellular localization of Arabidopsis *MDL proteins*

We previously performed *in silico* analysis of the three MDL proteins regarding the presence of subcellular targeting signals. This revealed a putative nuclear localization signal for MDL1 and a predicted C-terminal peroxisomal targeting sequence (PTS1) for MDL3 (20). Proteomic studies further reported MDL1 and MDL2 as being stromal chloroplast proteins (25, 26) and MDL3 as being a peroxisomal protein (27, 28). Accordingly, the Arabidopsis Cell electronic Fluorescent Pictograph (eFP) Browser at BAR ePlant (https://bar.utoronto.ca/eplant/) presents MDL1 and MDL2 preferably localizing to chloroplasts and MDL3 to peroxisomes (Fig. S2).

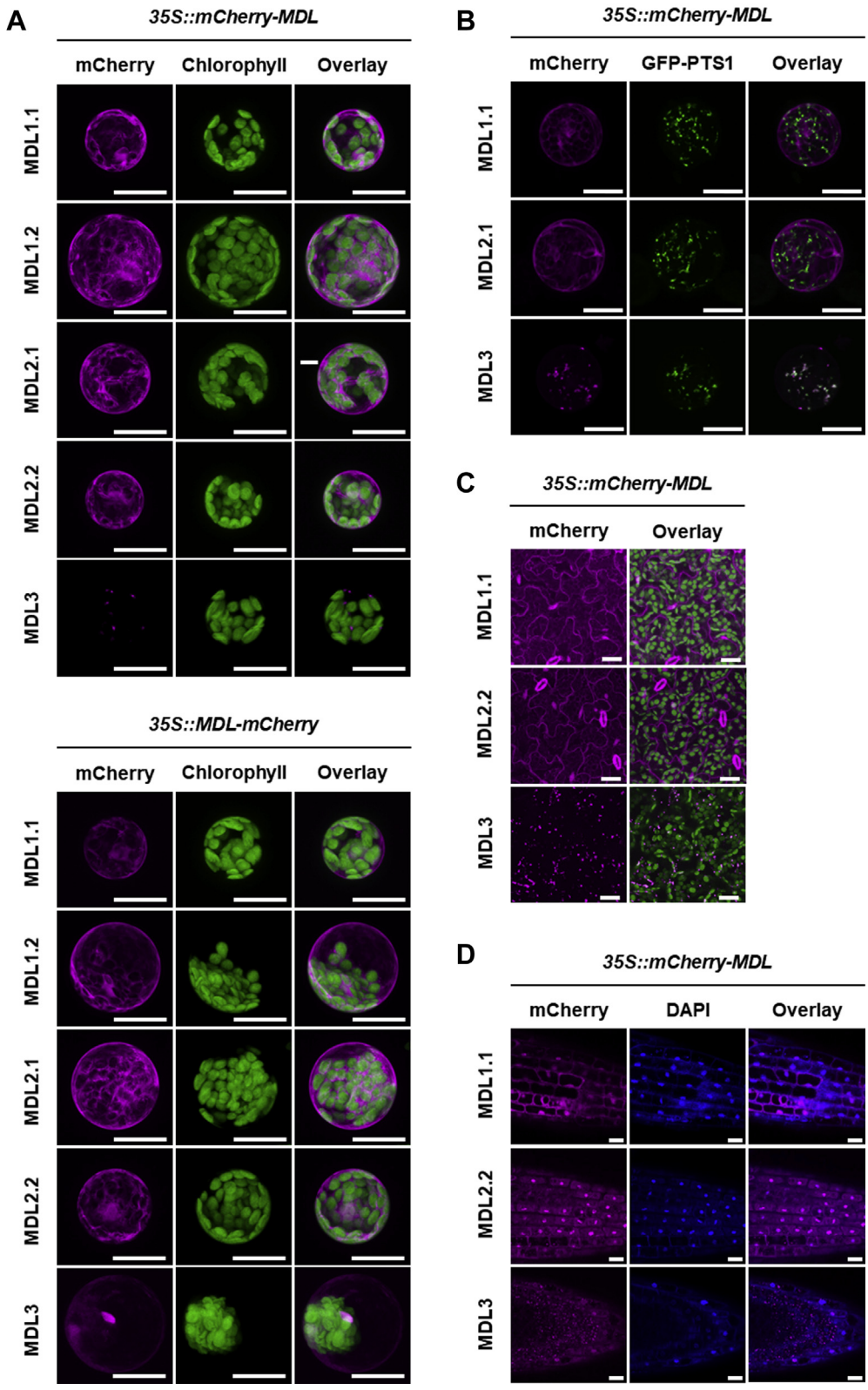

Figure 1. Subcellular localization of MDL proteins. *A*, transient expression of N-terminally (*upper part*) and C-terminally (*lower part*) mCherry-tagged MDL fusion proteins in *Arabidopsis* mesophyll protoplasts. Imaging was performed by CLSM. From left to right: mCherry signal displayed in *magenta*; chlorophyll autofluorescence shown in *green*; overlay of mCherry and autofluorescence signals. *B*, transient expression of N-terminally mCherry-tagged MDL fusion proteins in *Arabidopsis* mesophyll protoplasts derived from a transgenic GFP-PTS1 reporter line. Imaging was performed by CLSM. From *left* to *right*: mCherry signal displayed in *magenta*; GFP signal shown in *green*; overlay of mCherry and GFP signals. *C*, subcellular localization of N-terminally mCherry-tagged MDL fusion proteins in leaf epidermis and mesophyll cells, stably and constitutively expressed in three-week-old seedlings of respective transgenic lines. Imaging was performed by CLSM. *Left*: mCherry signal displayed in *magenta*; *right*: overlay of mCherry (*magenta*) and chlorophyll autofluorescence (*green*) signals. *D*, subcellular localization of N-terminally mCherry-tagged MDL fusion proteins in root tip cells, stably and constitutively expressed in

To explore the subcellular localization of the MDLs experimentally, we generated N- and C-terminally mCherry-tagged variants and expressed these transiently in *Arabidopsis* leaf mesophyll protoplasts under the control of the constitutive cauliflower mosaic virus 35S promoter. We recorded mCherry fluorescence and chlorophyll autofluorescence in transformed protoplasts by confocal laser scanning microscopy (CLSM). This revealed mainly cytoplasmic and frequently nuclear localization of MDL1 (both MDL1.1 and MDL1.2) and MDL2 (both MDL2.1 and MDL2.2), irrespective of the site of tagging (N- or C-terminal). We further noted a punctate mCherry fluorescence pattern for the N-terminally tagged MDL3 fusion protein and nucleocytoplasmic localization for the C-terminally tagged MDL3 variant. No mCherry-derived fluorescence was observed in chloroplasts, which could be unequivocally identified by their characteristic chlorophyll-mediated autofluorescence, for any of the MDL fusion proteins (Fig. 1*A*). Colocalization of mCherry-MDL3 with a canonical peroxisomal marker (GFP-PTS1; (29)) upon transient expression in leaf mesophyll protoplasts derived from a transgenic GFP-PTS1 marker line supports residence of the MDL3 fusion protein in peroxisomes (Fig. 1*B*).

We next generated transgenic lines stably expressing N-terminally mCherry-tagged MDL variants (MDL1.1, MDL2.2, and MDL3) under the control of the viral 35S promoter in the background of *Arabidopsis* accession Col-0. CSLM analysis of rosette leaves of these lines revealed a similar pattern of subcellular MDL localization as in the leaf mesophyll protoplasts, with the mCherry-MDL1.1 and mCherry-MDL2.2 fusions localizing to the cytoplasm and partly the nucleus and mCherry-MDL3 locating to mobile punctate structures, likely representing peroxisomes. Again, we did not detect any of the fluorophore-tagged MDLs in chloroplasts (as identified by their autofluorescence; Fig. 1*C*). CLSM-based imaging of root tips of the same transgenic lines in combination with labeling of nuclei *via* the fluorescent DAPI (4′,6-diamidino-2-phenylindole) dye further corroborated nucleo-/cytoplasmic localization of mCherry-tagged MDL1.1 and MDL2.2 and likely peroxisomal localization of MDL3 (Fig. 1*D*).

Arabidopsis *MDLs form homo- and hetero-oligomeric complexes*

To identify *in vivo* protein interaction partners of MDL proteins, we first performed a yeast two-hybrid (Y2H) screen using the three MDLs as bait proteins. For this and all following protein interaction experiments, we limited our analysis to the prevalent MDL1.1 and MDL2.1 splice variants (Fig. S1*E*), referred to as MDL1 and MDL2 in the following. The screen was performed in an automated manner on a one-by-one basis against a prey library (full-length ORFeome) of *Arabidopsis* comprising 12,000 full-length cDNAs (30). This yeast-based approach yielded MDL1 and MDL2 (preys) as interaction partners of MDL1 (bait), MDL1 (prey) as an interaction partner of MDL2 (bait), and PEX5 (AT5G56290), a protein of unknown function (AT5G64160), as well as a cysteine/histidine-rich C1 domain family protein (AT2G42060) (preys) as interaction partners of MDL3 (bait). We subsequently validated these candidate interactions identified in the high-throughput screen by targeted one-on-one Y2H analysis (Fig. 2*A*). In summary, these data suggest that MDL1 has the capacity to form homo-oligomers, whereas MDL1 and MDL2 might also form hetero-oligomers. Consistent with its peroxisomal localization and the presence of a C-terminal PTS1 targeting signal, MDL3 interacted with the PTS1 receptor PEX5. Its second interacting protein, AT5G64160, lacks any recognizable protein domains but was already found previously as an interactor of MDL3 (31).

In the following, we focused on the putative homo- and hetero-oligomerization of the MDLs by exploring all possible pairwise interactions between the three proteins using three different *in planta* experimental approaches. As a first approach, we used the split luciferase assay, which is based on the complementation of N- and C-terminal luciferase fragments translationally fused to the proteins of interest. Successful establishment of luciferase activity by fragment complementation can be assessed quantitatively by luminometric measurements. We transiently coexpressed the three MDLs N-terminally tagged with cLuc (C-terminal luciferase fragment) and nLuc (N-terminal luciferase fragment) in *Nicotiana benthamiana* and scored the resulting luminescence. This revealed noticeable luciferase activities upon coexpression of cLuc-MDL1 in combination with nLuc-MDL1 and nLuc-MDL2, cLuc-MDL2 in combination with nLuc-MDL1 and nLuc-MDL2, as well as cLuc-MDL3 in combination with nLuc-MDL2 and nLuc-MDL3. Accordingly, the respective pooled luminescence intensity values of multiple experimental replicates differed in a statistically significant manner from empty vector controls, which was not the case for the other tested pairwise combinations (Fig. 2, *B* and *C*).

As a second approach, we transiently coexpressed epitope-tagged (FLAG and mCherry) versions of various combinations of the three MDLs in *N. benthamiana* and performed co-immunoprecipitation (co-IP) assays using epitope-directed antibodies. This revealed pull-down of mCherry-MDL1 together with FLAG-MDL1 and FLAG-MDL2, of mCherry-MDL2 together with FLAG-MDL1, as well as of mCherry-MDL3 together with FLAG-MDL3 (Fig. 2*D*).

Finally, as a third approach, we took advantage of the transgenic *Arabidopsis* Col-0 lines constitutively expressing one of the three mCherry-tagged MDLs (Fig. 1*C*) and a monoclonal antibody directed against MDL2 (designated ATM 20C8; Fig. S3*A*) to perform co-IP experiments under seminative conditions in *Arabidopsis* leaf extract. This procedure yielded pull-down of mCherry-MDL1 together with MDL2 as well as mCherry-MDL2 (here MDL2.2) together with MDL2 (Fig. 2*E*). In summary, data of four independent protein interaction assays (Y2H, split luciferase, co-IP in

five-day-old seedlings of respective transgenic lines. Imaging was performed by CLSM. From left to right: mCherry signal displayed in *magenta*; DAPI signal shown in blue; overlay of mCherry (*magenta*) and DAPI (*blue*) signals. Images shown in (*A–C*) are maximum projections of z-stacks, micrographs shown in (*D*) represent one focal plane. Scale bars represent 25 μm.

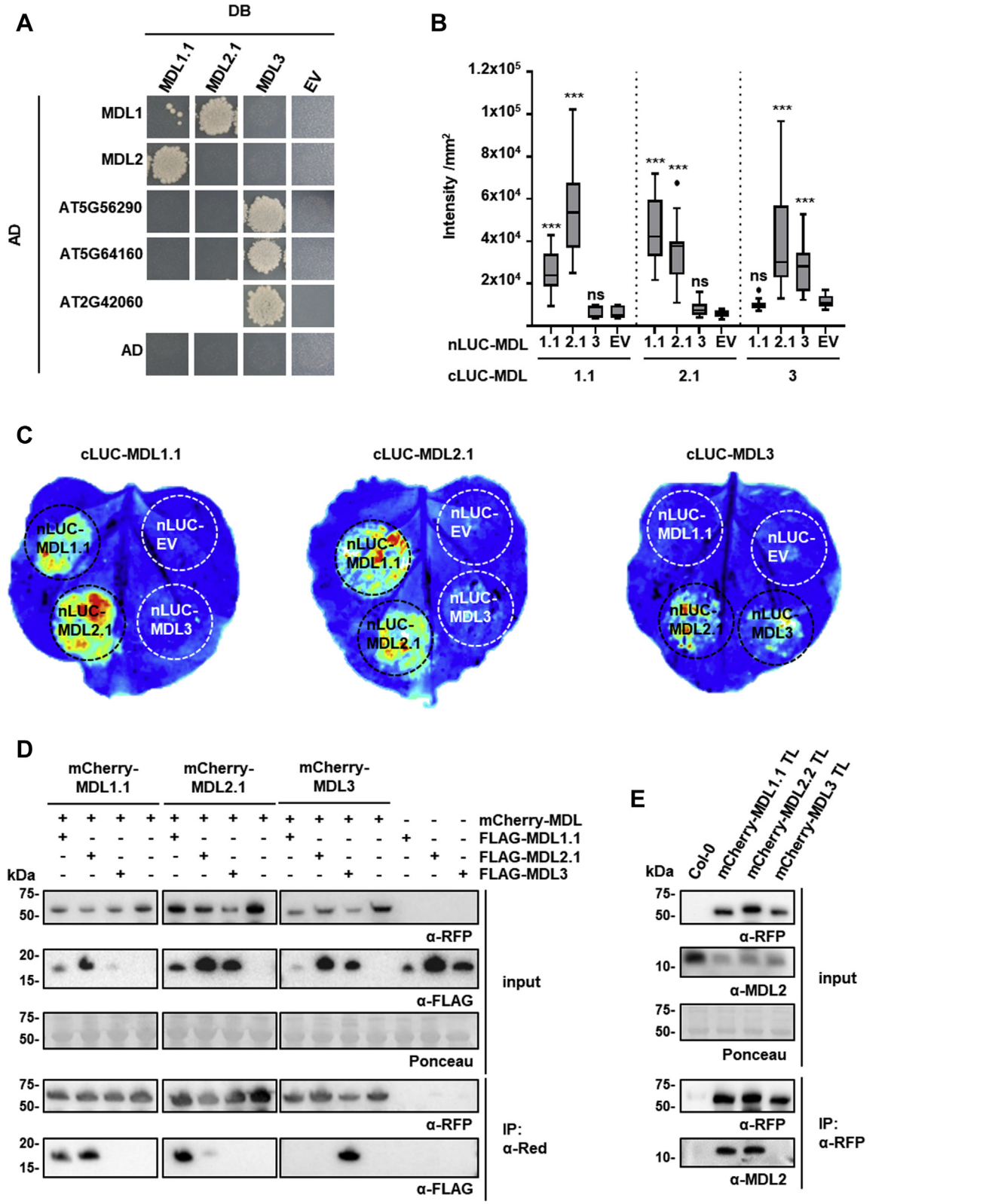

Figure 2. *Arabidopsis* MDL proteins form homo- and in part hetero-oligomeric complexes. *A*, Y2H assay. Candidate interactions of a previous high-throughput screen were validated by pairwise one-on-one matings using DNA-binding domain (DB) DB-MDL1, -MDL2, and -MDL3 or empty vector (EV) as bait for prey activation domain (AD)-tagged candidate interactors, including EV. Interactions were assayed by growth on selective plates using the HIS3 reporter. The experiment was performed three times with similar results. *B* and *C*, split-luciferase assay. cLUC-MDL1, -MDL2, and -MDL3 were transiently co-expressed with nLUC-MDL1, -MDL2, and -MDL3 or nLUC-EV (empty vector) in *N. benthamiana*. At 1 day post inoculation (dpi) (for cLUC-MDL1 combinations) or 2 dpi (for cLUC-MDL2 and cLUC-MDL3 combinations), plants were sprayed with 1 mM luciferin for the detection of luminescence. *B*, Quantification of data from the split-luciferase complementation assay. The luminescence of four independent experiments was quantified and is shown as a *boxplot*. Statistical significance between the interactions of the three MDLs and the EV control was determined with a two-way multipaired ANOVA test

Table 1
Summary of *MDL* protein–protein interaction data[a]

Protein 2	Protein 1		
	MDL1	MDL2	MDL3
MDL1	Y2H: (yes) co-IP (*Nb*): yes split luc: yes	Y2H: yes co-IP (*Nb*): yes split luc: yes	Y2H: no co-IP (*Nb*): no split luc: no
MDL2	Y2H: yes co-IP (*Nb*): yes split luc: yes co-IP (*At*): yes	Y2H: no co-IP (*Nb*): (yes) split luc: yes co-IP (At): yes	Y2H: no co-IP (*Nb*): no split luc: yes co-IP (At): no
MDL3	Y2H: no co-IP (*Nb*): no split luc: no	Y2H: no co-IP (*Nb*): no split luc: no	Y2H: no co-IP (*Nb*): yes split luc: yes

[a] Y2H, yeast two-hybrid assay; co-IP (*Nb*), co-immunoprecipitation in *N. benthamiana*; split luc, split luciferase assay; co-IP (*At*), co-immunoprecipitation in *A. thaliana*. Protein 1 refers to the MDL bait protein in Y2H analysis, the mCherry-tagged MDL protein in co-IP, and the nLuc-tagged MDL protein in the split luciferase assay. Protein 2 refers to the MDL prey protein in Y2H analysis, the FLAG-tagged MDL protein in co-IP (*Nb*), the cLuc-tagged MDL protein in the split luciferase assay, and the endogenous MDL2 protein in co-IP (*At*). Yes, clear interaction; (yes), weak interaction; no, lack of detectable interaction.

N. benthamiana, and co-IP in *Arabidopsis*) in essence consistently indicate MDL1-MDL1, MDL1-MDL2, and MDL2-MDL2 interactions (Table 1). Moreover, results from split luciferase and co-IP experiments in *N. benthamiana* further suggest MDL3-MDL3 interactions. These data are thus indicative of the *in planta* formation of MDL1, MDL2, and MDL3 homo-oligomers as well as the formation of MDL1-MDL2 hetero-oligomers.

A collection of Arabidopsis mdl *mutants for functional assays*

We selected a range of T-DNA insertion lines for the three *MDL* genes in the background of the accession Col-0 from various *Arabidopsis* stock collections. For each *MDL* gene, we obtained two homozygous mutant alleles (Table 2). Qualitative RT-PCR analysis revealed that the respective *mdl1* and *mdl2* mutants lack any detectable transcript and thus are likely to be null mutants. By contrast, we found lower but still noticeable transcript accumulation in the two *mdl3* mutants, indicating that these are rather knockdown than knockout mutants (Fig. S4).

To account for potential functional redundancy of the three *MDL* genes, we additionally generated double and triple mutants based on the six available T-DNA mutants by inter-mutant crossings. This resulted in two independent *mdl* triple mutants with distinctive allele combinations (*mdl1*-1 *mdl2*-2 *mdl3*-3 and *mdl1*-2 *mdl2*-1 *mdl3*-2) and a set of respective *mdl* double mutants (Table S1). Immunoblot analysis of these mutants using the above-mentioned α-MDL2 monoclonal antibody ATM 20C8 revealed the absence of detectable MDL2 protein in leaf extracts of the two *mdl2* single mutants and all double and triple mutants harboring these mutations. Further, we did not observe any compensatory MDL2 hyper-accumulation in any of the *mdl1* and/or *mdl3* single and double mutants (Fig. S3*B*). All single, double, and triple *mdl* mutants had a wild-type-like appearance and did not show any conspicuous abnormalities during the vegetative growth phase (Fig. S5, double mutants not shown).

Arabidopsis mdl *mutants exhibit a delayed flowering phenotype*

During the crossing procedure and propagation of the *mdl* mutants, we noticed that some of these appeared to initiate flowering later than isogenic Col-0 wild-type plants. To explore this potential mutant phenotype systematically and to discriminate a putative general delay in plant development from a delayed switch from vegetative to reproductive growth, we performed experiments under controlled conditions. In these experiments, we included, apart from the Col-0 wild-type, mutants *short vegetative phase*-41 (*svp*-41; (32)) and *constans*-10 (*co*-10 (33)), which are known for early and late flowering, respectively, as additional controls. We grew the two *mdl* triple mutants and the respective single mutants both under short- (8 h light; SD) and long-day (16 h light; LD) conditions and scored the total number of leaves (rosette plus cauline leaves) upon bolting as an indirect readout of flowering time. Under LD conditions, Col-0 wild-type plants had a median number of 15 leaves when transitioning to flowering, similar to previous reports (32). Control mutants *svp*-41 and *co*-10 showed the expected early and late flowering phenotypes in LD conditions, with a median of 8 and 53 leaves, respectively. Both *mdl* triple mutants differed in leaf numbers in a statistically significant manner from Col-0 wild-type, with medians of 23 (*mdl1*-1 *mdl2*-2 *mdl3*-3) and 21 (*mdl1*-2 *mdl2*-1 *mdl3*-2) leaves, respectively. The values of the six corresponding *mdl* single mutants were in a similar range as for the two triple mutants, though in tendency somewhat lower, but still significantly different from Col-0 wild-type according to statistical analysis (Fig. 3, *A* and *B*). Under SD conditions, on the other hand, the various *mdl* single and triple mutants showed a similar number of leaves at the transition from vegetative to reproductive growth as Col-0 plants and *co*-10 mutant plants (median of 65–81 leaves; no statistically significant difference). Only *svp*-11 mutants still flowered earlier (median of 21 leaves; Fig. 3*C*), as expected. In summary, the *mdl* mutants exhibit a consistent photoperiod-dependent delayed flowering phenotype, which is most pronounced in the two triple mutants and weaker but still recognizable in the six single mutant lines.

(***$p < 0.001$, ns = not significant). Raw data and exact statistical values for this graph can be found in in the supplemental source data file (Supporting file 1). *C*, Representative photographs of *N. benthamiana* leaves and the emitted luminescence (from *blue* = *low* to *red* = *high*). *D*, co-immunoprecipitation of epitope-tagged MDLs. FLAG-MDL1, -MDL2, and -MDL3 and mCherry-MDL1, -MDL2, and -MDL3 were transiently coexpressed in *N. benthamiana*. At 2 dpi, proteins were extracted and immunoprecipitation was performed for the mCherry-MDL proteins using α-RFP agarose (capturing mCherry). mCherry-MDL proteins were detected with an α-RFP antibody and FLAG-MDL proteins with a monoclonal α-FLAG antibody. Ponceau staining was used as a loading control. Co-immunoprecipitation was repeated twice with similar results. *E*, *in planta* protein-protein interaction of MDL2. Three-week-old transgenic *Arabidopsis* seedlings stably expressing mCherry-MDL fusion proteins (transgenic lines; "TL") were used for the immunoprecipitation of mCherry-MDL proteins using α-RFP agarose. mCherry-MDLs were detected with an α-RFP antibody and MDL2 was detected with the monoclonal α-MDL2 antibody ATM 20C8. Ponceau staining was used as a loading control. Co-immunoprecipitation was repeated twice with similar results.

Table 2
A collection of *mdl* mutants for functional assays

AGI identifier	Gene name	Mutant	T-DNA line	Site of insertion
AT5G57170	*MDL1*	*mdl1*-1	SAIL_772_G01	Exon 2
		mdl1-2	GK_786_B08	Intron 2
AT5G01650	*MDL2*	*mdl2*-1	SALK_024488C	Intron 1
		mdl2-2	SALK_078883	Intron 2
AT3G51660	*MDL3*	*mdl3*-2	SM_3_31346	3' untranslated region
		mdl3-3	GK_750_H06	Intron 1

Arabidopsis mdl *mutants possess unaltered infection phenotypes to adapted and nonadapted powdery mildew fungi*

Given that *MDL3* is coexpressed with several key components of plant defense (20), we suspected that at least *mdl3* mutants might play a role in the plant response to pathogens. We thus challenged *mdl* mutants with various plant pathogens to reveal whether they show any altered infection phenotype. We first inoculated the two sets of *mdl* mutants (single and triple mutants) with conidiospores of the fungus

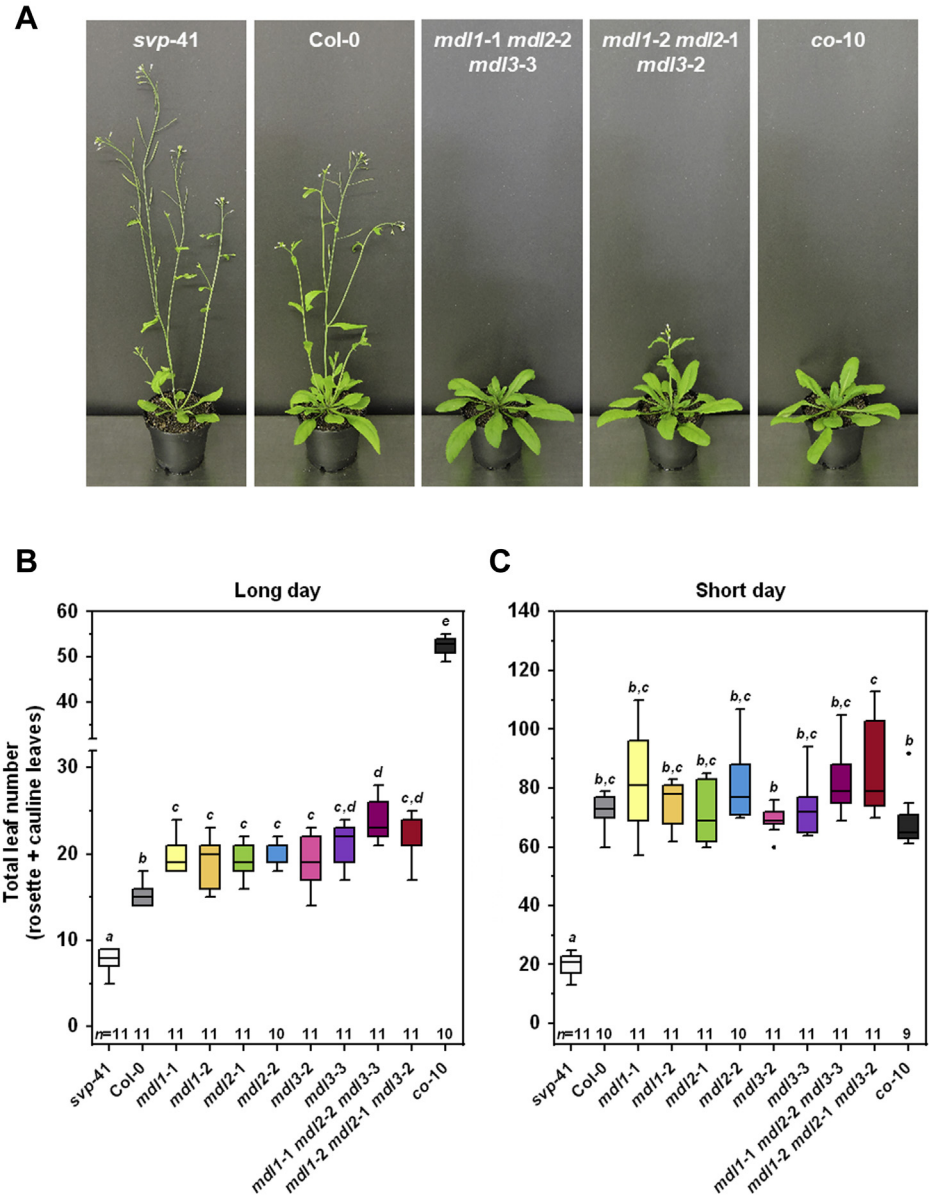

Figure 3. *Arabidopsis mdl* mutants exhibit a delayed flowering phenotype. *A*, flowering phenotype in LD conditions (16 h light) of two 42-day-old *mdl1 mdl2 mdl3* triple mutants in comparison to Col-0 wild-type and the flowering mutants *svp*-41 (early) and *co*-10 (late). *B* and *C*, flowering time as indicated by the total leaf number at the time of bolting of the indicated *mdl* single and triple mutants in comparison to Col-0 wild-type and the flowering mutants *svp*-41 and *co*-10 grown in LD (16 h light; *B*) or SD (8 h light; *C*) conditions. *Boxplots* represent 9–11 evaluated plants per genotype as given as *n* above the x-axis. Statistical significance between the plant genotypes was determined with a one-way multipaired ANOVA test. Letters above the boxplots denote different significance groups ($p < 0.05$). The experiment was repeated at least four times in LD conditions with similar results. The experiment in SD conditions was performed once. Raw data and exact statistical values for these two graphs can be found in in the supplemental source data file (Supporting file 1).

Golovinomyces orontii, which is an adapted powdery mildew pathogen of *Arabidopsis* (34). The resulting macroscopically visible infection phenotype (white powder-like fungal conidiation) was comparable for Col-0 and the tested *mdl* mutants at 7 days post inoculation (dpi) (Fig. S6*A*). Similarly, the microscopically assessed host cell entry rates of *G. orontii* conidiospores at 48 hours post inoculation (hpi) were similar for Col-0 wild-type plants and the two *mdl* triple mutants (median of 88–91%; no statistically significant difference; Fig. S6*B*). By contrast, the highly resistant *mlo2 mlo6 mlo12* control mutants (35, 36) allowed very low levels of host cell entry (median of 0–2%; Fig. S6*B*) and lacked the characteristic signs of fungal sporulation (Fig. S6*A*), as expected.

Since *MDL3* is coexpressed with genes that play a key role in resistance to nonadapted pathogens such as *PEN2* (37) and *PEN3* (38) and because MDL3, like PEN2, localizes to peroxisomes (Fig. 1*B*; (37)), we also tested the outcome of interactions between *mdl* mutants and the nonadapted barley powdery mildew pathogen, *Blumeria graminis* f.sp. *hordei* (*Bgh*). Col-0 wild-type plants had a median *Bgh* host cell entry rate of 10%, while the *pen2*-1 mutant, which is defective in nonhost resistance, allowed 34% (median) penetration by *Bgh*. All six tested *mdl* single mutants showed similar host cell entry rates as Col-0 (median of 8–13%, no statistically significant difference to Col-0; Fig. S6*C*).

Arabidopsis mdl *mutants exhibit enhanced basal resistance to* Pseudomonas syringae *pv.* maculicola

Next, we explored the infection phenotype of the *mdl* mutants upon challenge with the bacterial pathogen *P. syringae* pv. *maculicola* strain ES4326 (*Psm*), which is virulent on *Arabidopsis*. For this purpose, we took advantage of a strain that carries a chromosomal integration of the *Photorhabdus luminescens* luciferase gene (here designated as *Psm lux*). This strain is well established and allows to assess bacterial propagation by measuring the luminescence emitted from infected leaves (39, 40). We infiltrated bacterial suspensions in rosette leaves of five-week-old Col-0 wild-type and *mdl* mutant plants and scored the macroscopic infection phenotype and resulting luminescence at 3 dpi. We observed the characteristic *Psm*-induced leaf chlorosis in Col-0 plants, while we noticed reduced disease symptoms (chlorosis and water-soaked lesions) in the case of the *mdl* triple mutants (Fig. 4*A*). This correlated well with a strongly (approximately tenfold) reduced luminescence (*i.e.*, bacterial propagation) in the *mdl* triple mutants as compared with Col-0. The bacteria-derived luminescence of the six corresponding *mdl* single mutants was intermediate, *i.e.*, lower than in the case of Col-0 but higher than in the respective *mdl* triple mutants (Figs. 4*B* and S7).

In addition to the enhanced basal resistance phenotype of *mdl* mutants with *Psm* in local leaves, *MDL3* shows characteristics of genes potentially involved in systemic acquired resistance (SAR), an induced form of resistance in systemic tissue after local infections with (hemi-)biotrophic pathogens (41). These features comprise (i) increased transcript levels of *MDL3* (but not *MDL1* or *MDL2*) in systemic leaf tissue of *Arabidopsis* Col-0 in the course of biologically induced SAR, and (ii) induction of *MDL3* transcript accumulation by pipecolic acid (a precursor of the key SAR signaling molecule *N*-hydroxy-pipecolic acid) application in a FLAVIN-DEPENDENT MONOOXYGENASE1 (FMO1)-dependent manner ((42, 43); Fig. S8*A*). We therefore also explored a potential deficiency of *mdl3* mutants to develop SAR. To this end, we infiltrated primary (local) leaves of Col-0 and *mdl3* mutant plants with either buffer ($MgCl_2$, mock control) or *Psm*, which is a potent inducer of SAR (44). Two days later, we challenged systemic leaves with *Psm lux* and determined bacterial luminescence in these leaves at 3 dpi. This experiment revealed a strong reduction in bacterial titers in the systemic leaves of all plants that were inoculated with *Psm* bacteria in local leaves. Since there was no detectable difference between Col-0 wild-type plants and the two tested *mdl3* mutants, we conclude that *mdl3* mutants retain the capacity to induce SAR (Fig. S8*B*). The reduced bacterial luminescence in the mock-treated *mdl3* mutant plants in comparison to Col-0 wild-type nevertheless further corroborated the enhanced resistance of *mdl3* mutants to *Psm* (cf. Figs. 4*B* and S7).

Enhanced basal resistance of Arabidopsis mdl *mutants to* Psm *is compromised by additional mutation of the salicylic acid biosynthesis gene* SID2

Salicylic acid (SA) is a key phytohormone that orchestrates the plant immune response to various pathogens, including bacteria (45). We thus hypothesized that SA might be involved in the enhanced disease resistance of the *mdl* mutants. To test this proposition experimentally, we took advantage of genetic analysis by crossing the *mdl1*-1 and *mdl3*-2 single mutants as well as the *mdl1*-1 *mdl2*-2 *mdl3*-3 triple mutant with the *sid2*-1 mutant, which is defective in the gene encoding isochorismate synthase 1, a key enzyme in salicylic acid biosynthesis (46, 47). We challenged homozygous *mdl1*-1 *sid2*-1 and *mdl3*-2 *sid2*-1 double mutant as well as *mdl1*-1 *mdl2*-2 *mdl3*-3 *sid2*-1 quadruple mutant plants and respective controls (Col-0, *sid2*-1) with *Psm lux* by leaf infiltration and recorded the resulting bacterial luminescence at 3 dpi. The outcome of this assay recapitulated in tendency the enhanced resistance phenotype of *mdl1*-1, *mdl3*-2, and *mdl1*-1 *mdl2*-2 *mdl3*-3 (Fig. 5, *A* and *B*, cf. Fig. 4) and revealed the expected supersusceptibility phenotype of the *sid2*-1 mutant (46). Consistently, all genotypes harboring the *sid2*-1 mutation in addition to the *mdl* alleles showed the typical *Psm* disease symptoms (Fig. 5*A*) and permitted bacterial proliferation at levels similar to *sid2*-1 plants (Fig. 5*B*; *mdl1*-1 *sid2*-1 and *mdl3*-2 *sid2*-1 not shown). These data indicate that the *sid2*-1 mutation is genetically epistatic to the *mdl* mutations. They further suggest that the enhanced resistance phenotype of *mdl* mutants might depend on the defense-based accumulation of the signaling molecule SA.

Given that according to genetic analysis SA contributes to the enhanced bacterial resistance of *mdl* mutants, we wondered whether the accumulation of SA and/or other relevant signaling and defense-associated molecules would be altered in these mutants following pathogen challenge. We thus determined the

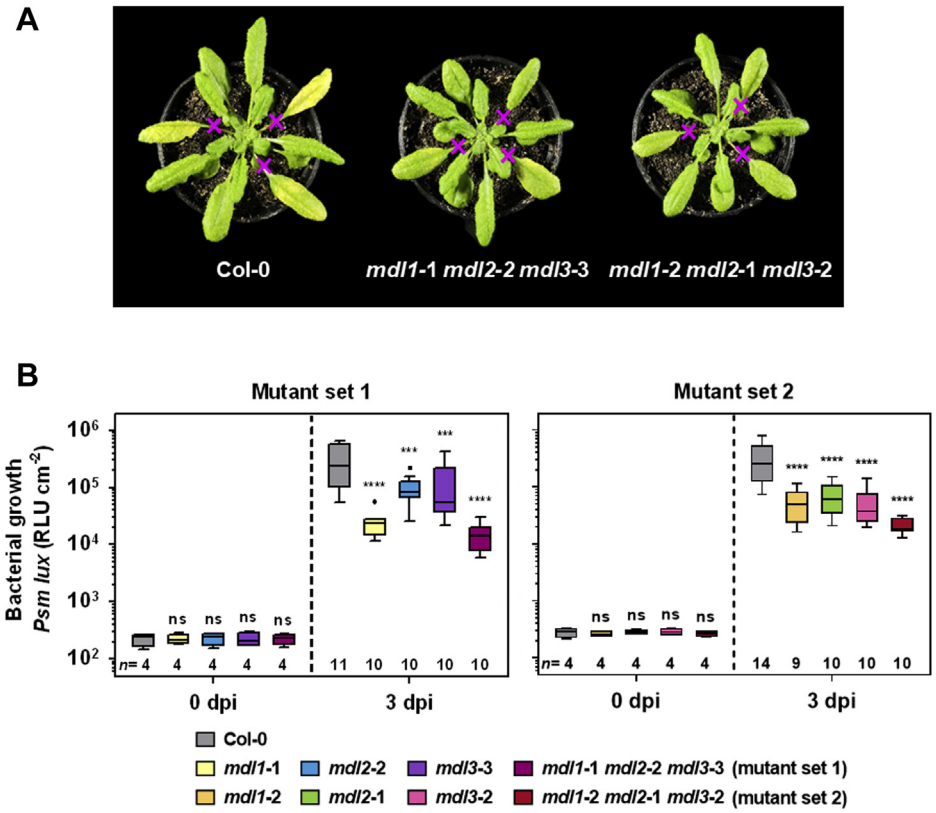

Figure 4. *Arabidopsis mdl* mutants exhibit enhanced basal resistance to *Psm*. Three mature leaves of five-week-old *Arabidopsis* plants were infiltrated with *Psm lux* (OD_{600} 0.0005). *A*, representative macroscopic disease phenotypes of two *mdl1 mdl2 mdl3* triple mutants in comparison to Col-0 wild-type at 3 dpi. Crosses in magenta mark the inoculated leaves. *B*, *Boxplots* represent bacterial titers of *Psm lux* at 0 dpi and 3 dpi in leaves from the indicated *mdl* single and triple mutants of the two *mdl* mutant sets in comparison to Col-0 wild-type. Titers were quantified *via* bacterial bioluminescence and are given as relative light units (RLU) cm^{-2}. The number of evaluated plants per genotype and time point is given as *n* above the x-axis with each plant value representing the mean of three leaves. Statistical significance between the plant genotypes was determined for the 0 dpi and 3 dpi datasets, each in comparison to the respective Col-0 control, with a two-way multipaired ANOVA test (****$p < 0.0001$, ***$p < 0.001$, **$p < 0.01$, ns = not significant). Shown is data of one representative experiment per mutant set of at least three independent biological replicates of each set with similar results. Raw data and exact statistical values for this graph can be found in in the supplemental source data file (Supporting file 1). Data of additional experimental repetitions are given in Fig. S7.

levels of total SA, jasmonic acid-isoleucine (JA-Ile), *N*-hydroxypipecolic acid (NHP), abscisic acid (ABA), camalexin, indole-3-carboxylic acid (ICA), and some others in the rosette leaves of Col-0 control plants, two *mdl1* single mutants, and both *mdl* triple mutants. The respective leaf samples were collected in mock-treated and *Psm*-inoculated plants at 32 hpi. We found a strong increase of total SA, NHP, ABA, camalexin, and ICA as well as a marked decrease of JA-Ile upon bacterial inoculation, but did not notice any statistically significant difference between the genotypes tested. Likewise, we did not observe any constitutive accumulation or depletion of any of these molecules in the mock-treated *mdl* mutants as compared with Col-0 wild-type plants (Figs. 5*C* and S9). Taken together, the enhanced disease resistance phenotype of *mdl* mutant plants does not correlate with any detectable differences in the constitutively present and inducible levels of the signaling and defense metabolites analyzed.

Bacterial infection induces changes in Arabidopsis MDL *transcript and protein levels and triggers subcellular relocalization of MDL proteins*

With the aim to characterize the role of the MDL genes/proteins during bacterial pathogenesis further, we next studied transcript and protein accumulation in time-course experiments upon *Psm* challenge. In accordance with publicly accessible microarray data (http://bar.utoronto.ca/efp/cgi-bin/efpWeb.cgi), semiquantitative RT-PCR revealed opposite trends for *MDL1* and *MDL2* on the one hand and *MDL3* on the other hand, with reduced transcript levels of *MDL1* (from 12 hpi onwards) and *MDL2* (at 48 hpi) and an increase in *MDL3* transcript levels (from 12 hpi onward; Fig. S10). Immunoblot analysis with the monoclonal α-MDL2 antibody, which does not cross-react with bacterial proteins (Fig. S11*A*), indicated a putative moderate increase (approximately twofold) in MDL2 protein abundance at later time points during *Psm* infection (at 24 hpi and 48 hpi; Fig. S11*B*).

To find out whether bacterial colonization would result in a change of subcellular protein localization, we analyzed leaf samples of seedlings of the above-mentioned transgenic lines stably expressing mCherry-MDL1.1, mCherry-MDL1.2 mCherry-MDL2.2, and mCherry-MDL3 (Fig. 1, *C* and *D*) upon spray challenge with *Psm* by CLSM. We observed the seemingly erratic formation of prominent cytoplasmic MDL1.1 and MDL1.2 (and to a lesser degree also MDL2.2) protein aggregates at the peripheral lobes of leaf epidermal cells following bacterial infection (Fig. 6*A*). Plasmolysis with 1 M $MgCl_2$

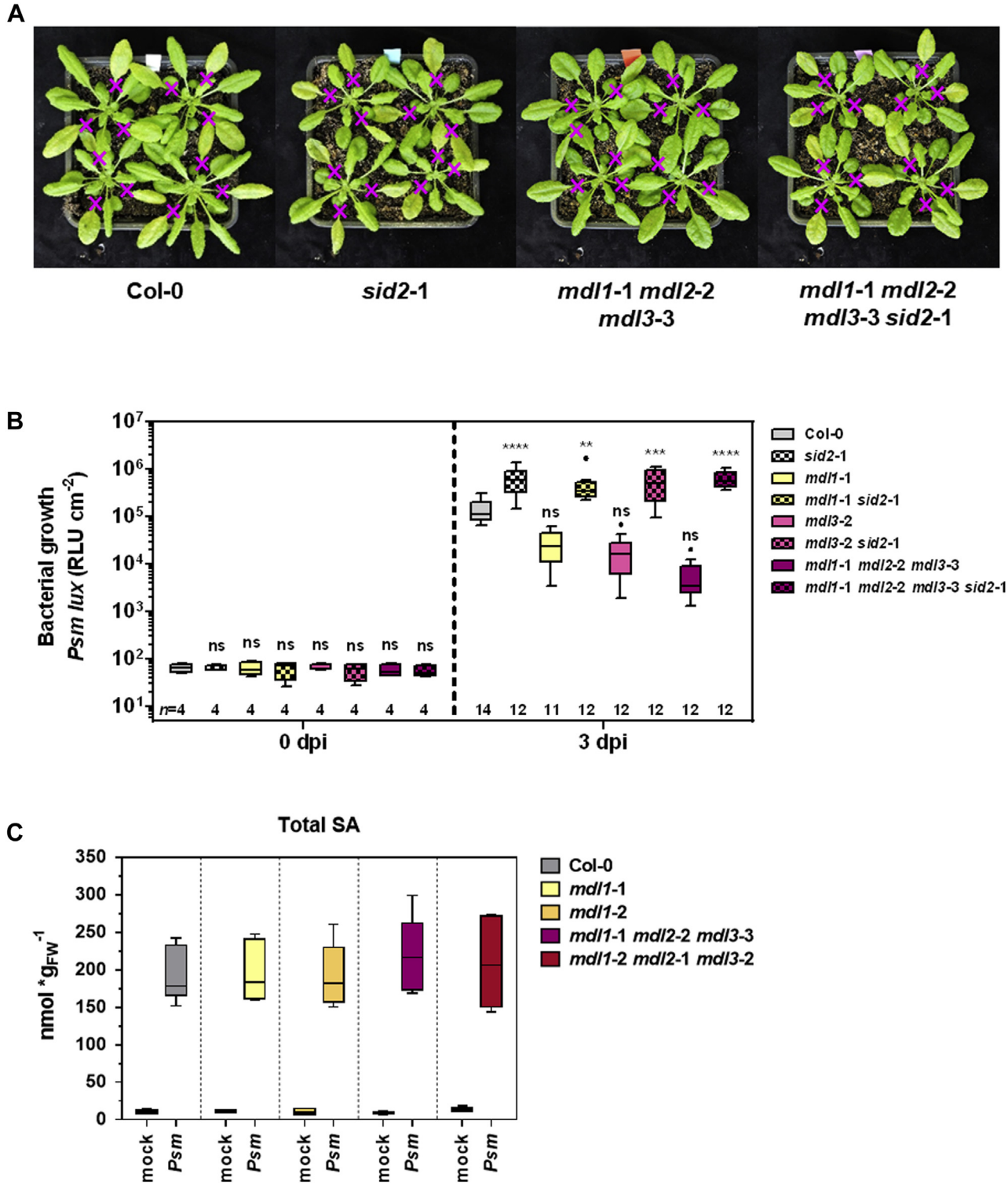

Figure 5. Enhanced disease resistance of the *Arabidopsis mdl* mutants to *Psm* depends on SA biosynthesis but is associated with unaltered SA levels. *A* and *B*, three mature leaves of five-week-old *Arabidopsis* plants were infiltrated with *Psm lux* (OD_{600} 0.0005). *A*, representative macroscopic infection phenotypes at 3 dpi of Col-0 wild-type, *sid2*-1, *mdl1*-1 *mdl2*-2 *mdl3*-3 triple, and *mdl1*-1 *mdl2*-2 *mdl3*-3 *sid2*-1 quadruple mutant plants. Crosses in magenta mark the inoculated leaves. *B*, *boxplots* represent bacterial titers of *Psm lux* at 0 dpi and 3 dpi in leaves of *mdl1*-1 and *mdl3*-2 single as well as *mdl1*-1 *mdl2*-2 *mdl3*-3 triple mutants in comparison to Col-0 wild-type, the *sid2*-1 single mutant, *mdl1*-1 *sid2*-1 and *mdl3*-2 *sid2*-1 double mutants as well as the *mdl1*-1 *mdl2*-2 *mdl3*-3 *sid2*-1 quadruple mutant. Titers were recorded *via* bacterial bioluminescence and are given as RLU cm^{-2}. The number of evaluated plants per genotype and time point is given as *n* above the x-axis with each plant value representing the mean of three leaves. Statistical significance between the plant genotypes was determined for the 0 dpi and 3 dpi datasets, each in comparison to the respective Col-0 control, with a two-way multipaired ANOVA test (****$p < 0.0001$, ***$p < 0.001$, **$p < 0.01$, ns = not significant). Shown are data from one representative experiment of two independent biological replicates with similar results. Raw data and exact statistical values for this graph can be found in in the supplemental source data file (Supporting file 1). *C*, local levels of total SA at 32 hpi in leaves of two independent *mdl1* single and two independent *mdl1 mdl2 mdl3* triple mutants and Col-0 wild-type following infiltration with *Psm* (OD_{600} 0.005) or buffer (10 mM $MgCl_2$, mock control). *Boxplots* represent data from two independent biological replicates

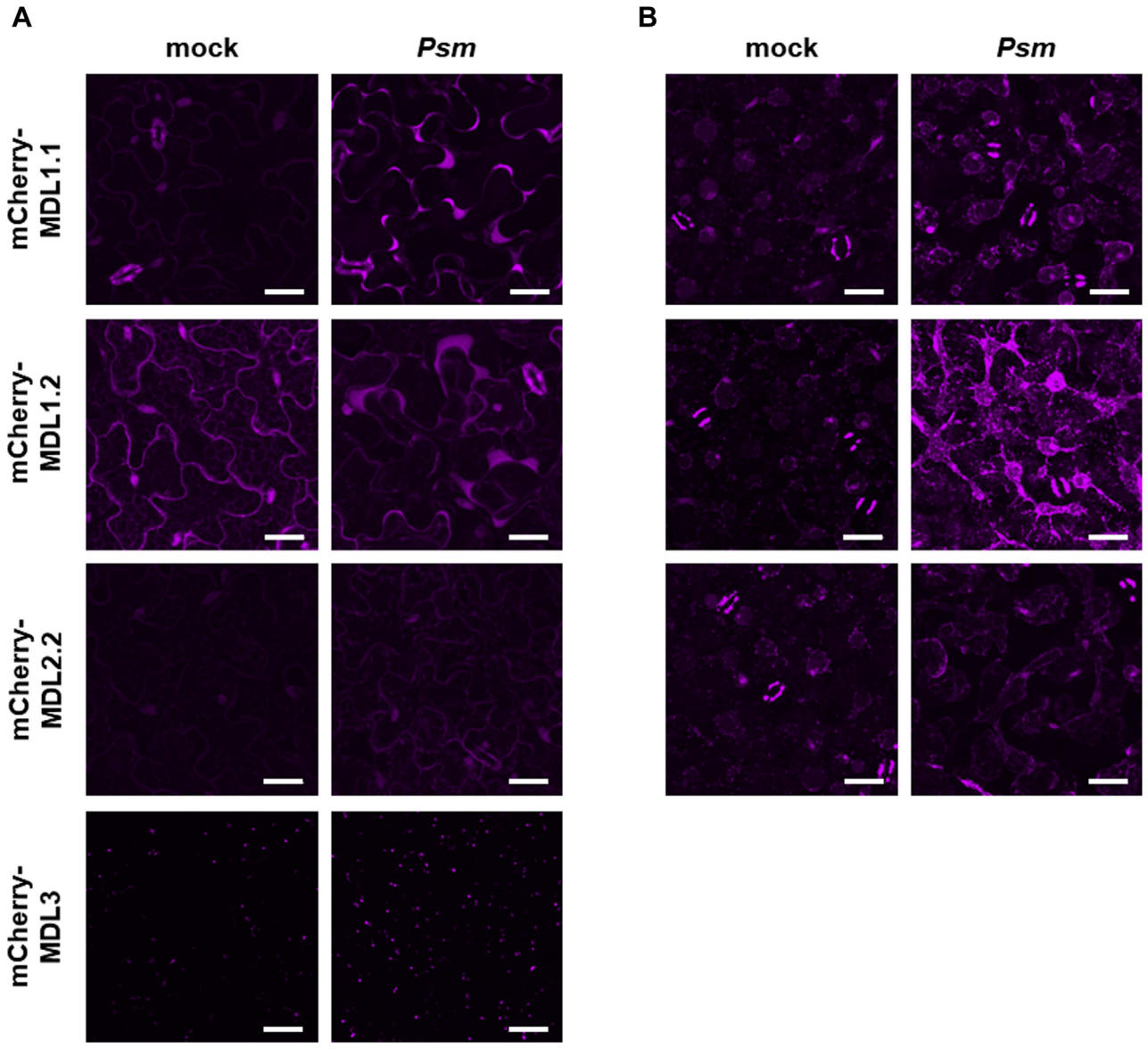

Figure 6. Subcellular relocalization of stably expressed mCherry-tagged MDL proteins in response to *Psm* infection. *A*, three-week-old transgenic *Arabidopsis* seedlings stably expressing N-terminally mCherry-tagged MDL fusion proteins were spray-inoculated with *Psm* (OD_{600} 0.2) or mock-treated (10 mM $MgCl_2$). Displayed are subcellular localizations of mCherry-MDL fusion protein in leaves (epidermal and mesophyll cells) determined by CLSM at 2 dpi. *B*, seedling leaves from (*A*) after treatment with 1 mM $MgCl_2$ for the induction of plasmolysis. All images shown are maximum projections of z-stacks. Scale bars represent 25 µm.

resulted in retraction of the fluorescent signal from the cell walls, which suggests that these aggregates were indeed formed in the cytoplasm and are not present in the extracellular (apoplastic) space (Fig. 6*B*). This is consistent with the finding that in immunoblot analysis the vast majority of the MDL2 pool appears to be intracellular following *Psm* challenge, with only a weak or no signal in apoplastic washing fluids (Fig. S12). In summary, these experiments provide evidence for transcriptional and posttranscriptional *MDL* dynamics upon bacterial infection.

Discussion

MIF and MIF-like proteins such as D-DT have been studied primarily in humans and animals (1, 3, 16) and in some of their unicellular pathogens, *e.g.*, members of the genera *Plasmodium* and *Leishmania* (19, 48). It has been shown that these protists deliver their own MIF variants into their hosts to interfere with immune signaling by impeding host MIF functionality (49–51). Similarly, the release of aphid MIFs into a plant host has been demonstrated to modulate plant immunity (24). Apart from the latter report, a comprehensive *in silico* analysis (20),

with three technical replicates each (six values in total). Statistical significance between the plant genotypes was determined for the mock-treated and *Psm*-challenged plants, each in comparison to the respective Col-0 control, with a two-way multipaired ANOVA test (ns = not significant). Raw data and exact statistical values for this graph can be found in in the supplemental source data file (Supporting file 1).

recombinant protein work (21, 52), and phylogenetic studies (18), plant MIF proteins have not been subject to functional investigation, in particular not in their native organismal context. Despite the sequence-relatedness to their human counterparts, MDL proteins thus belong to the still large group of *Arabidopsis* proteins with yet unknown biochemical and biological function (53). Here we provide a basic experimental characterization of the *Arabidopsis* MDL gene/protein family, revealing a contribution of the three MDLs in this plant species to the modulation of bacterial infection and the control of flowering time.

We investigated the subcellular localization of the three *Arabidopsis* MDLs by expressing fluorophore-tagged protein variants both transiently in *Arabidopsis* leaf mesophyll protoplasts (Fig. 1, *A* and *B*) and stably in transgenic lines (Fig. 1, *C* and *D*). Both approaches yielded consistent results—nucleo-cytoplasmic localization of MDL1 and MDL2 irrespective of the site of protein tagging (N- or C-terminal) and peroxisomal localization of N-terminally tagged MDL3. Peroxisomal localization of MDL3 in our studies is in line with previous observations (27, 28, 54) and the presence of a canonical C-terminal peroxisomal targeting sequence (PTS1). Accordingly, masking of the C-terminal PTS1 sequence by a C-terminal fluorophore-tag results in nucleo-cytoplasmic instead of peroxisomal localization (Fig. 1*A*). The low molecular mass below the nuclear size exclusion limit of approximately 60 kDa may allow passive diffusion of cytosolic MDL1 and MDL2 into the nucleus. Human MIF has been found to be actively transported into the nucleus by the protein apoptosis-inducing factor in neurons undergoing hypoxic or excitotoxic stress (14), raising the possibility that comparable processes might be operative in plants as well. Overall, we assume that the detection of MDL1 and MDL2 in former chloroplast proteomic studies (25, 26) might be due to cytoplasmic contaminations in the chloroplast preparations or the "stickiness" of MDL proteins to these organelles.

Four different types of protein–protein interaction assays indicate homo- and hetero-oligomerization of the three *Arabidopsis* MDL proteins (Table 1). The few discrepancies between the outcomes with individual assays could be due to (1) the type, position, and length of the tags used to analyze the interactions, (2) the lack of expression of particular constructs in a given system, (3) unfavorable conditions for the interaction in the nucleus (Y2H), or (4) the lack of required post-translational modifications in the yeast system (Y2H). Particularly MDL1 and MDL2 seem to have the capacity to form homo-oligomers on the one hand as well as MDL1-MDL2 hetero-oligomers on the other hand (Fig. 2 and Table 1). Human MIF crystallizes as a noncovalent homotrimer. An MIF trimer is required for the tautomerase activity of MIF since the catalytic cavity is jointly formed by residues from different subunits, and it is the trimer that is believed to bind to the MIF receptor CD74 and to represent the physiologically relevant form (55–57). The subunit–subunit interfaces within the human MIF trimer have been characterized by an intertwining loop structure. This interaction comprises prominent contributions from residues 38–44 and 96–102 of β-strands 2 and 5, respectively, as well as of the central β-sheet of one subunit, and from residues 48–50 and 107–109, respectively, from two adjacent subunits, which extend the 4-stranded central β-sheet into a 6-stranded sheet structure (55). However, cross-linking experiments performed under physiological concentrations of human MIF in solution have suggested that MIF oligomeric species may dynamically change between monomeric, dimeric, and trimeric forms. In addition, MIF engagement of its chemokine receptors CXCR2 and CXCR4 has been suggested to occur at low nanomolar concentrations at which the monomer would be the favored species (6, 10). Although an *in silico* comparison insinuates also a trimeric structure for the MDLs (20, 21), their specific oligomeric species *in planta* remains unclear.

Besides MDL-MDL interactions, no other proteins were identified as interaction partners of MDL1 or MDL2 in an Y2H screen. This might indicate that these two proteins do not require further partners. However, it must be taken into account that only about 48% of *Arabidopsis* genes are represented by the screened ORFeome and that the employed Y2H implementation has a documented assay sensitivity of ∼35% (31). In the case of MDL3, the peroxisomal import receptor PEX5 was identified as an interactor, which is consistent with the presence of a peroxisomal PTS1 import signal and subcellular localization of MDL3 in peroxisomes. The additional two proteins found in the Y2H screen (AT2G42060 and AT5G64160) will need to be validated by *in planta* approaches in future studies. Finally, targeted interaction studies might be performed with known interactors of human MIF that are also present in plants, such as the COP9 signalosome subunit CSN5/JAB1 or the redox proteins peroxiredoxin-1 and superoxide dismutase-1 (3).

We obtained homozygous T-DNA knockout mutants for genes *MDL1* and *MDL2* and respective *mdl1 mdl2* double knockout lines (Table 2 and Table S1), which are all transcript null mutants (Fig. S4). At least for the *mdl2* mutants also the respective protein is undetectable (Fig. S3*B*). These findings indicate that *MDL1* and *MDL2* are dispensable in *Arabidopsis*, both individually and in combination, for growth and reproduction. By contrast, the available *mdl3* mutants with T-DNA insertions in an intron and in the 3' untranslated region retained residual transcript levels (Fig. S4). We thus currently do not know whether *MDL3* is an essential gene in *Arabidopsis* that results in lethality when fully inactivated.

We discovered that the *mdl* mutants possess a delayed flowering phenotype in LD conditions, which was most pronounced in the two independent *mdl1 mdl2 mdl3* triple mutant lines (Fig. 3). This phenotype is apparent under LD conditions but not in SD settings. It will require extensive additional studies (*e.g.*, genetic epistasis analysis with well-characterized flowering time mutants) to place the MDL proteins more precisely in the complex network of pathways controlling flowering time in various environments (58).

We found that *mdl* mutants exhibit unaltered infection phenotypes in response to adapted and nonadapted powdery mildew fungi (Fig. S6) but enhanced disease resistance to the bacterial pathogen *Psm* (Fig. 4). Enhanced disease resistance in plant

mutants is frequently the consequence of autoimmunity, *i.e.*, a constitutive activation of plant defense prior to pathogen challenge, which is typically correlated with retarded plant growth (dwarfism) and/or the occurrence of spontaneous cell death in leaf tissue ("lesion mimic mutants"; (59)). At the molecular level, such mutants also often show constitutive expression of defense marker genes and/or the accumulation of defense signaling molecules in the absence of any pathogen (60–62). However, *mdl* mutants have a normal growth habit (Fig. S5) and lack recognizable lesions and detectable changes in the level of defense-associated phytohormones and metabolites in unchallenged plants. The tested molecules also do not hyperaccumulate upon bacterial infection (Figs. 5*C* and S9). We thus conclude that the increased disease resistance of *mdl* mutants to *Psm* is unlikely to be due to constitutive defense or the enhanced activation of common defense pathways. The observed supersusceptibility of *mdl sid2* mutants (Fig. 5*B*) might thus not indicate SA dependence of the *mdl* resistance phenotype but hint to the SA-dependent defense sector acting in parallel to the MDL pathway(s). We, therefore, hypothesize that the MDL proteins could rather serve as host susceptibility factors for *P. syringae* bacteria that might be targeted by conventional or unconventional bacterial effector proteins. Precedence for such effector-targeted susceptibility factors exists in various plant pathosystems (63–67). These susceptibility factors might be in turn guarded by cytoplasmic plant immune sensors, and the absence of their guardees could result in their inappropriate activation and thus enhanced disease resistance (67). As an alternative scenario we cannot rule out that MDL proteins act as negative regulators of noncanonical plant defense responses.

In the human system, recombinant MIF protein has been described to enhance biofilm formation of *Pseudomonas aeruginosa*, an opportunistic bacterial pathogen with a broad host range that is distantly related to *Psm* (68). Biofilm formation could promote bacterial infection and thus explain the proposed role of MDLs as host susceptibility factors. Although also the phytopathogen *P. syringae* has the capacity to form biofilms (69), this is, however, an unlikely scenario for the *Arabidopsis–Psm* interaction since *Psm* bacteria remain localized extracellularly during plant colonization, and no evidence was found for the secretion of MDL proteins during bacterial pathogenesis (Figs. 6*B* and S12).

Bacterial challenge triggers subcellular relocalization of transgenically expressed and fluorophore-tagged MDL1 and MDL2, resulting in its aggregation at the peripheral lobes of epidermal cells (Fig. 6*A*). Recruitment of plasma membrane-localized defense-related proteins to sites of attempted entry has been reported for powdery mildew fungi (70, 71). This response can be recapitulated by the exogenous application of conserved pathogen elicitors such as the flg22 epitope or chitin (72). It depends on cytoskeleton function and intracellular protein trafficking (73). We are, however, not aware of any reports describing similar protein redistribution upon bacterial infection, especially considering the nucleo-cytoplasmic (nonmembrane) localization of MDL1 and MDL2. Unlike the situation for human MIF (3, 8), our experimental data do not support pathogen-triggered secretion of MDL proteins to the extracellular space (Figs. 6*B* and S11). The physiological relevance of the change in subcellular localization thus remains to be explored.

It is noteworthy that both mutant phenotypes discovered in this study—*i.e.*, enhanced resistance to *Psm* and delayed flowering—are detectable in all *mdl* single mutants (including the *mdl3* mutants that still retain residual transcript levels; Fig. S4) and exacerbated in the respective *mdl* triple mutants. This finding points to the notion that all three MDL proteins may cofunction in the same cellular pathway where they might act in partial redundancy. Such a scenario could be reconciled most easily with all three proteins cooperating within the same protein complex, with a protein assembly lacking one paralog being less active. However, while the three *MDL* genes are coexpressed in rosette leaves, they show nonoverlapping expression patterns in other plant organs (20). Moreover, the distinctive subcellular localization of MDL1 and MDL2 (nucleo-cytoplasmic; Fig. 1) on the one hand and MDL3 (peroxisomal; Fig. 1) on the other hand, as well as the lack of convincing evidence for physical interaction between MDL1/MDL2 and MDL3 (Fig. 2 and Table 1), argue against this hypothesis. Nonetheless, at least in rosette leaves, the MDL proteins might act as nonessential components in consecutive steps of a given cellular pathway.

Some plant mutants that exhibit both an altered flowering time and immune phenotype have been described. An example is the elevated level of resistance to the fungal pathogen *Fusarium oxysporum* seen in late-flowering mutants and the significant correlation of late flowering and enhanced disease resistance in natural *Arabidopsis* accessions. The respective study identified the photoperiodic pathway flowering time regulator GIGANTEA as a susceptibility factor for *F. oxysporum* infection (74). By contrast, mutants defective in the transcriptional regulator gene *MED18* show late flowering in combination with enhanced susceptibility to fungal (*Botrytis cinerea* and *Alternaria brassicicola*) infection (75). In addition, in particular mutants with deficiencies in the biosynthesis or signaling pathways of defense-associated phytohormones (SA, JA-Ile, and ethylene) exhibit both deregulated plant immunity and altered flowering time. Examples comprise SA mutants such as *sid2* and *eds5* (76), the JA-Ile receptor mutant *coi1* (77), and ethylene-insensitive mutants such as *etr1*, *ein2*, and *ein3* (78). The MDL proteins are novel players that likewise modulate both the control of plant immunity and flowering time. The mechanistic details of how these three proteins engage in the cross talk between these two processes remain to be explored. The elucidation of these specifics may feed back to the human system, where intracellular MIF functions remain poorly understood. This research may thus also bring about new insights into pathomechanisms underlying human diseases, thereby closing the loop of cross-kingdom MIF studies.

Experimental procedures

Plant material and growth conditions

All *Arabidopsis* lines used in this study (Table S1) are in the genetic background of accession Columbia-0 (Col-0). T-DNA

insertion mutants in *MDL* genes were obtained from the European Arabidopsis Stock Centre (NASC; http://arabidopsis.info). Homozygous individuals of the T-DNA insertion lines were confirmed as recommended (79) using the T-DNA left border and gene-specific primers (see Table S2). Mutants homozygous for the *sid2*-1 point mutation (46) were identified *via* a cleaved amplified polymorphism (CAPS) marker by restriction of the respective polymerase chain reaction (PCR) fragment with *Mfe*I. Double and higher-order mutants were obtained by intermutant crossings. All mutant lines were finally confirmed through DNA sequencing of the respective PCR amplicons.

Arabidopsis seeds were stratified, sown in an 8:1:1 mixture of soil (ED73, Balster Einheitserdewerk GmbH, Fröndenberg, Germany; sterilized by 10 min microwaving before use), sand, and vermiculite, and placed in controlled short- (SD) or long-day (LD) conditions. Two weeks after seeding, seedlings were individually transplanted into bigger pots, either singly in small pots of 6 cm diameter or as 1–4 plants per 9 × 9 × 8 cm pots depending on the purpose. Plants for flowering experiments, crossings, and seed production were grown in a 16 h light/8 h dark LD cycle at 20 °C, a relative humidity of 60–70%, and with a photon flux density of 80–100 μmol m^{-2} s^{-1}. Plants for all other experiments were generally grown in SD cycles of 10 h light/14 h dark or of 8 h light/16 h dark in the case of flowering experiments, 20 °C, 60–70% relative humidity, and 80–100 μmol m^{-2} s^{-1} photon irradiance.

N. benthamiana plants were grown in SoMi513 soil (HAWITA, Vechta, Germany) in 9 × 9 × 8 cm pots in a 10 h light/14 h dark SD cycle at 20 °C, 80–90% relative humidity, and a light intensity of 80–100 μmol m^{-2} s^{-1}. Plants infiltrated with *A. tumefaciens* were transferred to an LD cycle of 16 light at 23 °C/8 h dark at 20 °C, 60–65% relative humidity, and a light intensity of 105–120 μmol s^{-1} m^{-2}.

Cloning

Coding sequences of *MDL1.1*, *MDL1.2*, *MDL2.1*, *MDL2.2*, and *MDL3* were cloned *via* GATEWAY Cloning Technology (Invitrogen, Carlsbad, CA, USA) into the respective entry (pDONR207) and destination vectors. The destination vectors used in this study are summarized in Table S2.

The destination vectors p35S::mCherry-GWY and p35S::GWYmCherry were generated by introducing the amplified mCherry PCR product into pExHisHA *via* either restriction sites *Eco*RI and *Sma*I or *Sma*I and *Xba*I, respectively. The GWY cassette was introduced into the recombinant p35S::mCherry vector by using the restriction site *Sma*I. The destination vectors pAMPAT-cLUC-GWY and pAMPAT-nLUC-GWY were generated by introducing either cLUC-GWY or nLUC-GWY from pCAMBIA-cLUC-GWY or pCAMBIA-nLUC-GWY (80), respectively, into pAMPAT-MCS-*Sac*I *via* the restriction sites *Hind*III and *Sac*I. pAMPAT-MCS-*Sac*I is a derivative of pAMPAT-MCS (GenBank accession number AY436765.1) and was generated by introducing a synthesized DNA fragment containing the restriction site *Sac*I *via* *Hind*III and *Nco*I.

Gene expression analysis by reverse transcriptase–polymerase chain reaction (RT-PCR)

Total RNA was extracted from rosette leaves of *Arabidopsis* plants using the NucleoSpin RNA Plus kit (Macherey-Nagel, Düren, Germany) following the instructor's manual. One microgram of total RNA was treated with DNase I (Sigma-Aldrich, Merck KGaA, Darmstadt, Germany) prior to the reverse transcription into cDNA using the High-Capacity RNA-to-cDNA kit (Applied Biosystems, Invitrogen, Carlsbad, CA, USA) following the manufacturer's instructions. The resulting cDNA was diluted 1:10 before application in PCR. RT-PCR was performed as a standard application with GoTaq G2 DNA Polymerase using 2.5 μl of diluted cDNA per 50 μl reaction. Gene AT4G26410 was used as a reference gene (81). The respective primer pairs used for RT-PCR are listed in Table S3.

Transient gene expression *in* Arabidopsis *protoplasts*

Transfection of *Arabidopsis* mesophyll protoplasts was performed by the tape-sandwich method (82). Leaves of five-week-old *Arabidopsis* plants were fixed with the upper epidermal surface on autoclave tape. Subsequently, the lower epidermal surface was ripped off with the help of Tesa tape. Leaves were placed peeled in an enzyme solution containing cellulose OnozukaTM R-10 and macerozymeTM R-10 (both Yakult, Tokyo, Japan) and incubated gently shaking at room temperature until cell walls were digested and mesophyll protoplasts distributed in the solution. The protoplast-containing solution was collected by centrifugation at 100 × *g* for 3 min at 4 °C, washed twice with 15 ml prechilled W5 (154 mM NaCl, 125 mM $CaCl_2$, 5 mM KCl, 5 mM glucose, and 2 mM MES, pH 5.7), and incubated on ice for 30 min. The protoplasts were collected by centrifugation at 100 × *g* for 3 min and subsequently resuspended in 4 ml MMG solution (0.4 M mannitol, 15 mM $MgCl_2$, and 4 mM MES, pH 5.7). For the transfection of protoplasts, 20 μl containing 7 μg of plasmid DNA was added to 200 μl of the prepared protoplasts. Subsequently, 220 μl PEG solution (40% (w/v) PEG 4000, 0.1 M $CaCl_2$, 0.2 M mannitol) was added, gently mixed, and incubated at room temperature for 10 min. Thereafter, the transfected protoplasts were washed trice with 0.9 ml W5 solution by centrifugation at 100 × *g* for 3 min. After the last washing step, the protoplasts were resuspended in 0.9 ml W5 and incubated in the dark overnight at room temperature.

Confocal laser scanning microscopy (CLSM)

For localization of fluorophore-tagged proteins, leaves of transgenic *Arabidopsis* seedlings were placed in a droplet of water on a glass slide and shielded with a coverslip. Analyses were performed with a Leica TCS SP8 lightning confocal microscope and the LAS-X software package (Leica Microsystems, Wetzlar, Germany). Pictures and z-stacks were recorded with a 20x water or 63x water immersion objective (Leica). For DAPI staining, seedlings were incubated in 1:500 diluted DAPI (AppliChem GmbH, Darmstadt, Germany) solution (DAPI stock solution 5 mg/ml in dimethylformamide

(Sigma-Aldrich)) for 2 h. Fluorescence signals were recorded in sequential scan mode with the following specifications: GFP excitation at 496 nm (argon laser) and emission at 499–523 nm; mCherry excitation at 561 nm (DPSS 561 diode) and emission at 589–622 nm; chlorophyll autofluorescence excitation at 476 nm and emission at 681–762 nm; DAPI excitation at 405 nm (Diode 405) and emission at 420–470 nm.

For the analysis of subcellular localization of fluorophore-tagged proteins after *Psm* inoculations, three-week-old SD-grown transgenic *Arabidopsis* seedlings were inoculated with *Psm* at an optical density OD at 600 nm (OD_{600}) of 0.2 or, for control, treated with 10 mM $MgCl_2$. Treatments were performed by spraying the solutions, each supplemented with 0.04 % v/v Silwet L-77 (Momentive Performance Materials GmbH, Leverkusen, Germany), twice from all sides. One day before and for 1 day after the treatment, the seedlings were covered with a lid to induce opening of the stomata in high humidity. Treated seedlings were analyzed by CLSM at 4, 24, and 48 hpi using the specifications given above.

Generation of transgenic Arabidopsis *plants*

Binary vectors with the open reading frames (ORFs) of *MDL1.1*, *MDL1.2*, *MDL2.1*, *MDL2.2*, and *MDL3*, N-terminally fused to mCherry, were introduced into *Arabidopsis* Col-0 wild-type plants through *A. tumefaciens*–mediated transformation by the floral dip method (83). *A. tumefaciens* strain GV3101 with the helper plasmid pMP90:RK was used for the transformation. T1 seedlings of T0 seeds recovered from the transformed plants were selected by spraying with BASTA solution (BASF, Ludwigshafen am Rhein, Germany). Sterilized T1 seeds resulting from BASTA-resistant T1 plants were individually seeded on MS plates containing BASTA. The developing T2 generation was screened for seedlings with an approximately 3:1 survival rate. T2 seeds, resulting from T2 plants with a 3:1 survival rate, were reassessed on BASTA-containing plates with MS medium to identify homozygous individuals (all seedlings survive). In addition, seedlings were checked for proper mCherry fluorescence. Homozygous individuals were multiplied and used in targeted applications.

Flowering time experiments

For the determination of the flowering time, *Arabidopsis* plants were stratified for uniform germination and grown under SD (8 h light/16 h dark) or LD (16 h light/8 h dark) cycles in controlled conditions. Uniform growth of the plants was followed by weekly counting the rosette leaves. The development of primary shoots was assessed by checking the plants every other day. Flowering time (in days) was scored when primary shoots reached 0.5 mm and was additionally assessed as the total number of rosette and cauline leaves of the main stem at the stage of full flowering.

Powdery mildew infection assays with G. orontii *and* B. graminis *f.sp.* hordei

Inoculation assays with *G. orontii* were performed with four-week-old *Arabidopsis* plants grown in SD conditions by leaf-to-leaf transfer of conidiospores using heavily infected leaves of *eds1*-2 [Col-0] mutant plants (84), which were the cultivation host for *G. orontii*. At 2 days post inoculation (dpi), leaf samples were collected from the infected target plants and placed in 80% (v/v) ethanol for the removal of leaf pigments. In the following, fungal structures were stained in a Coomassie solution (45% v/v methanol, 10% v/v acetic acid, 0.05% w/v Coomassie blue R-250; Carl Roth, Karlsruhe, Germany) for their visualization with a Zeiss Axiophot microscope (Carl Zeiss AG, Jena, Germany). Fungal host cell entry rates were quantified by the percentage of germinated fungal spores developing haustoria and secondary hyphae over germinated spores with restricted growth by plant formed appressoria. At least 100 germinated spores per leave (excluding stomatal and vessel regions) and four leaves per plant were evaluated to calculate a medium penetration success per plant. In addition, extra infected plants were evaluated at 7 dpi for their macroscopically visible disease symptoms.

Inoculation assays with *B. graminis* f.sp. *hordei (Bgh)* were performed as described before (85). In brief, four- to five-week-old *Arabidopsis* plants were inoculated by dusting off *Bgh* conidia from heavily infected barley plants. Subsequently, the inoculated *Arabidopsis* plants were transferred back to SD conditions. At 2 dpi, infected leaves were sampled and placed in 80% (v/v) ethanol for the removal of leaf pigments. In the following, fungal structures were stained in an aniline blue solution (150 mM K_2HPO_4, 0.01% w/v aniline blue; Sigma-Aldrich, Munich, Germany) for 1 day to visualize callose *via* fluorescence with an Axiophot microscope (Carl Zeiss AG, Jena, Germany), using UV excitation of 327–427 nm and a DAPI/aniline blue filter of 417–477 nm emission. Fungal host cell entry rates of *Bgh* were quantified by the percentage of inhibited penetration attempts (stained papilla) over successful penetration (haustorium inside the epidermal cell). At least 100 interaction sites were evaluated per leaf of three plants per genotype and experiment.

P. syringae *infection assays*

Bacterial infection assays were performed with *P. syringae* pv. *maculicola* ES4326 (*Psm*) and a *Psm* strain constitutively expressing the *P. luminescens luxCDABE* operon (*Psm lux*; (39). *Psm* and *Psm lux* were grown on King's B plates supplemented with 50 μg ml^{-1} rifampicin for *Psm* and *Psm lux* and 25 μg ml^{-1} kanamycin for *Psm lux* for 2 days at 28 °C. Overnight (log phase) liquid cultures in King's B medium were prepared from the plates, washed thrice in 10 mM $MgCl_2$, and diluted to the desired optical density in 10 mM $MgCl_2$.

For basal bacterial growth assays, three mature leaves of five-week-old SD-grown *Arabidopsis* plants of uniform and healthy appearance were infiltrated from the abaxial side with *Psm lux* at an OD_{600} of 0.0005 using a needleless 1 ml syringe. The bacterial growth in leaves was determined indirectly by recording the bacterial bioluminescence in leaf discs (r = 3 mm, adaxial side up) individually placed in 96-well microtiter plates (flat bottom) filled with 250 μl 10 mM $MgCl_2$. The

average bioluminescence was recorded for 10 s per well with a 10 s with the "Centro XS^3 LB 960 Microplate Luminometer" and the corresponding "MikroWin 2000 software" (Berthold Technologies, https://www.berthold.com/). Three leaf discs per plant were recorded and the average auto-luminescence (background of untreated leaves) was subtracted to determine the average bioluminescence per plant. Increasing luminescence values (given in relative light units, RLU) correlate linearly with increasing bacterial titers and reflect bacterial growth determined by the standard plate assay (39, 40).

For analyses of metabolites and protein accumulation after *Psm* inoculation, infiltrations were performed as described above except for using *Psm* at an OD_{600} of 0.005 for inoculations and 10 mM $MgCl_2$ as mock infiltrations. Leaf samples for metabolite analysis (six leaves per sample and three samples from six plants per genotype) were collected at 32 hpi. Leaf samples for protein analysis (two leaves from two plants per sample and three samples from six plants per genotype) were collected at 0, 2, 4, 6, 12, 24, and 48 hpi. In both cases, the samples were instantly shock-frozen in liquid nitrogen and stored at −80 °C for the following respective analysis.

SAR assays were carried out with five-week-old SD-grown *Arabidopsis* plants of healthy and uniform appearance. Three lower mature leaves were either infiltrated with *Psm* at an OD_{600} of 0.005 for inoculations or with 10 mM $MgCl_2$ as a mock treatment. Two days later, three upper (systemic) mature leaves of the same plants were challenged with infiltrations of *Psm lux* at an OD_{600} of 0.0005. The bacterial growth in the challenged leaves was determined 3 dpi *via* bioluminescence as described above.

Transient expression in N. benthamiana

A. tumefaciens (strain AGL1) harboring appropriate constructs and the GV2260 p19 helper strain were used for transient expression in *N. benthamiana* as described before (85) with minor modifications. In brief, bacterial cultures were resuspended in infiltration media (10 mM MES, pH 5.6, 10 mM $MgCl_2$, 200 μM acetosyringone) to an OD_{600} of 0.5 and incubated at room temperature for 2 h. For coinfiltration, equal volumes of each *A. tumefaciens* transformant were mixed and infiltrated with a needleless syringe from the abaxial side into fully expanded leaves of four to six-week-old *N. benthamiana* plants.

Protein isolation and immunodetection

For protein accumulation experiments, four leaves of different five-week-old *Arabidopsis* plants were homogenized in 200 μl protein extraction buffer (50 mM Tris pH 8.0, 1 mM EDTA, 1 mM DTT, 1 mM PMSF) and centrifuged for 20 min at 15,000 × *g* at 4 °C to remove cell debris. The protein concentration was determined using the Bradford protein assay (86). Unless otherwise stated, 5 μg total protein was used for the separation of proteins by sodium dodecylsulfate–polyacrylamide gel electrophoresis (SDS-PAGE). Each experiment was repeated at least once with similar results. Protein samples were denatured in 1xNuPAGE LDS Sample buffer (Thermo Fisher Scientific, Darmstadt, Germany) by boiling at 95 °C for 5 min prior to gel loading. Thereafter, samples were subjected to SDS-PAGE, transferred to a nitrocellulose membrane (0.2 μm, Carl Roth, Karlsruhe, Germany), and used for immunodetection according to the manufacturer's instructions. Primary antibodies were purchased from Chromotek (6G6, α-RFP, Planegg-Martinsried, Germany), Cell Signalling (D6W5B, α-FLAG, Frankfurt, Germany) or generated (20C8, α-MDL2, see below). Secondary antibodies were purchased from Cell Signalling (7074, α-rabbit IgG HRP, Frankfurt, Germany), Merck (A9037, α-rat IgG HRP, Darmstadt, Germany), and Thermo Fisher Scientific (32,430, α-mouse IgG HRP, Darmstadt, Germany). Chemiluminescence detection of antigen–antibody complexes was performed with SuperSignal West Femto Western substrate (Thermo Fisher Scientific, Darmstadt, Germany). As a loading control, nitrocellulose membranes were stained in Ponceau S (AppliChem GmbH, Darmstadt, Germany) solution. For protein accumulation after *Psm* inoculation, infiltrations were performed as described above, except for using *Psm* at an OD_{600} of 0.005 for inoculations and 10 mM $MgCl_2$ as mock infiltrations.

Generation of monoclonal α-MDL2 antibodies

For the production of MDL2-specific monoclonal antibodies, highly purified recombinant MDL2 protein was prepared using Rosetta (DE3)-competent *Escherichia coli* cells, which expressed a pET21-derived gene construct to yield a C-terminally 6xHis-tagged MDL2 (MDL2-6xHis) protein product. Bacterial expression and protein purification were carried out essentially as described previously (21, 52). Wistar rats were immunized with 60 μg purified full-length MDL2-6xHis, 5 nmol CpG (TIB MOLBIOL, Berlin, Germany) and an equal volume of Incomplete Freund's adjuvant (IFA; Sigma, St Louis, USA)). After a 6-week interval, a boost injection without IFA was given 3 days before the fusion of rat spleen cells with P3X63Ag8.653 myeloma cells using standard procedures (87, 88). Hybridoma supernatants were screened in a bead-based flow cytometry assay (iQue, Intellicyte; Sartorius, Göttingen, Germany). Briefly, MDL2-6xHis protein was captured to activated 3D Carboxy beads (PolyAN, Berlin, Germany) and incubated for 90 min with hybridoma supernatant and Atto 488-coupled isotype-specific monoclonal mouse-anti-rat IgG secondary antibodies. Antibody binding was analyzed using ForeCyt software (Sartorius, Göttingen, Germany). Positive supernatants were further assayed for their potential by western blot. Hybridoma cells from selected supernatants were subcloned at least twice by limiting dilution to obtain stable monoclonal cell lines. The experiments of this study were performed with the purified antibody clone ATM 20C8 (IgG2b/κ).

Yeast two-hybrid (Y2H) assays

Y2H screens were performed as described before (89). Briefly, ORFs encoding MDL1.1, MDL2.1, or MDL3 were

transferred by Gateway cloning from pDONR207 vectors into the GAL4 DNA-binding domain (DB)-encoding Y2H vector pDEST-pPC97, and subsequently transformed into the yeast strain Y8930. These constructs were screened by yeast mating against a collection of 12,000 *Arabidopsis* ORFs fused to the Gal4 activation domain (AD) in the yeast strain Y8800 (30). The screening was done as a binary mini-pool approach, *i.e.*, each DB-ORF was screened against pools of 188 AD-ORFs. Interactions were assayed by growth on selective plates using the *HIS3* reporter, adding 1 mM 3-amino-1,2,4-triazole (3-AT) to suppress background growth. This primary screen was carried out once and identities of candidate interactors were identified by Sanger sequencing. All candidate interactions were verified by pairwise one-on-one mating in three independent experiments. Only pairs scoring positive in all three assays were considered as *bona fide* interaction partners.

Co-immunoprecipitation

For co-IP, 500 µl of homogenized plant material (of two-week-old *Arabidopsis* seedlings or 2 dpi of transiently transformed *N. benthamiana*) was mixed with 1 ml extraction buffer (50 mM Tris-HCl, pH 8.0, 1 mM EDTA, 1 mM DTT, 1 mM phenylmethanesulfonyl fluoride (AppliChem GmbH, Darmstadt, Germany)) and centrifuged at 15,000 × *g* at 4 °C to remove cell debris. The protein concentration was determined using the Bradford protein assay and 500 µg of soluble proteins was incubated with 10 µl α-RFP-Trap Agarose slurry (ChromoTek GmbH, Planegg-Martinsried, Germany) for 1 h at 4 °C under constant agitation. Thereafter, beads were washed six times in 200 µl protein extraction buffer. After the last washing step, the protein extraction buffer was removed completely and the beads were resuspended in 50 µl SDS sample buffer. Briefly, before separation by SDS-PAGE, proteins were eluted by boiling the samples for 10 min at 95 °C.

Split luciferase complementation assays

For split luciferase complementation assays, transiently transformed leaves of *N. benthamiana* were sprayed with 1 mM D-luciferin (PerkinElmer, Rodgau, Germany) solved in water supplemented with 0.01% (v/v) Tween-20 at 2 days after infiltration. Leaves were kept in the dark for 10 min before luminescence was detected with a ChemiDoc XRS+ imagine system. Intensities/mm^2 of different combinations were evaluated using the Image Lab software (BioRad, Feldkirchen, Germany). For each combination of interaction partners, four independent experiments consisting of two different plants and two leaves per plant were evaluated.

Preparation and analysis of apoplastic wash fluid (AWF)

For the analysis of AWFs, five-week-old SD-grown *Arabidopsis* plants were sprayed with *Psm* or mock-treated (10 mM $MgCl_2$) as described above or left untreated. Four plants of each treatment and genotype were sampled at 24 and 48 hpi. To extract AWF, three leaves each of four to five *Arabidopsis* plants were cut and submerged in a beaker with infiltration buffer (20 mM MES, 2 mM $CaCl_2$, 0.1 M KCl, pH 6.0). To infiltrate, the beaker was placed in a desiccator, and a vacuum was applied for 5 min. After infiltration, the leaves were carefully padded dry and placed, the petiole facing up, in 1.5 ml tubes. The tubes were then centrifuged at 200 × *g* for 20 min at 4 °C. The AWF was collected from the bottom of the tubes and fluid from the same treatment was pooled. For leaf samples, two leaves from different plants were harvested and snap-frozen in liquid nitrogen. Protein was extracted from leaf samples as described above, with the addition of 0.1 % Tween to the extraction buffer. For immunoblotting, 10 µl of AWF or 7.5 µg of leaf protein was mixed with Laemmli buffer and denatured at 95 °C for 10 min. The samples were separated by SDS-PAGE, subsequently blotted onto a nitrocellulose membrane, and used for immunodetection as described above. In addition to α-MDL2, α-PsbA/D1 (AS05 084, PsbA/D1 protein of PS II, Agrisera, Vännas, Sweden) was used as a control for cytosolic contamination.

Analysis of phytohormones and defense-associated metabolites

Phytohormones were extracted with methyl-tert-butyl ether (MTBE), reversed phase-separated using an ACQUITY ultra performance liquid chromatography (UPLC) system (Waters Corp., Milford, MA, USA), and analyzed by nanoelectrospray ionization (nanoESI) (TriVersa Nanomate; Advion BioSciences, Ithaca, NY, USA) coupled with an AB Sciex 4000 QTRAP tandem mass spectrometer (AB Sciex, Framingham, MA, USA) employed in scheduled multiple reaction monitoring mode (90). The reversed phase separation of constituents was achieved by UPLC using an ACQUITY UPLC HSS T3 column (100 mm × 1 mm, 1.8 µm; Waters Corp., Milford, MA, USA). Solvents A and B were water and acetonitrile/water (90:10, v/v), respectively, both containing 0.3 mmol/l ammonium formate (adjusted to pH 3.5 with formic acid).

For absolute quantification of SA, SA glycoside (SAG), JA-Ile, NHP, ABA, camalexin, and ICA, the following internal standards were added to the plant material before extraction: 10 ng D_4-SA (C/D/N Isotopes Inc, Pointe-Claire, Canada), 50 ng $^{13}C_6$-SAG (kindly provided by Petr Karlovsky, Göttingen, Germany), 10 ng D_3-JA-Leu (kindly provided by Otto Miersch, Halle/Saale, Germany), 50 ng D_9-Pip (Merck KGaA, Darmstadt, Germany), 50 ng D_9-NHP (91), 10 ng D_6-ABA (C/D/N Isotopes Inc, Pointe-Claire, Canada), and 20 ng D_5-IAA (Eurisotop, Freising, Germany). Mass transitions and optimized parameters for the detection of these phytohormones and defense-associated metabolites by mass spectrometry are shown in Table S4. After data processing, the absolute amounts of SA and SAG were added to express the total SA levels.

Statistical analysis

In this study, "biological replicates" refers to data from fully independent experiments, whereas "technical replicates" refers to data from samples of the same experiment or plant. Statistical analyses and graph generation were performed using the GraphPad Prism software (GraphPad Prism Software Inc,

San Diego, CA, USA). In boxplot graphs, the center lines show the medians and upper and lower box limits indicate the 25th and 75th percentiles, respectively. Outliers are indicated by dots. Statistical analyses were performed using either a one-way analysis of variance (ANOVA) test or a two-way ANOVA test, in either case with Tukey's method for multiple comparisons (multipaired ANOVA) as indicated in the figure legends. Raw data and details of the statistical analysis for all figures can be found in the supplemental source data file (Supporting file 1).

Data availability

All data and materials are available upon request. Access to the monoclonal α-MDL2 antibody and the transgenic MDL lines requires a material transfer agreement (MTA).

Supporting information—This article contains supporting information (21, 32, 33, 37, 42, 43, 46, 52, 84, 35, 36).

Acknowledgments—We are grateful to George Coupland for providing flowering time mutants *co*-10 and *svp*-41. We thank Jane Parker for sharing plasmid vector pJawohl2b 3xFLAG-GWY. We acknowledge Karl-Heinz Kogel, Richard Bucala, Elias Lolis, Cornelia Herrfurth, and Lin Leng for constructive discussions.

Author contributions—R. P. and J. B. conceived the study. K. G., F. L., D. S., P. W., H. T., C. A., K. B., M. A., A. F., M. J., and K. Z. performed the experiments and analyzed the data. I. F., H. K., P. F.-B., R. F., J. B., and R. P. supervised the work. R. P. drafted the article. All the authors edited and reviewed the article.

Funding and additional information—This work was supported by the Deutsche Forschungsgemeinschaft (DFG, German Research Foundation)-Agence Nationale Recherche (ANR) co-funded project "X-KINGDOM-MIF - Cross-kingdom analysis of macrophage migration inhibitory factor (MIF) functions". Respective DFG grants are BE 1977/10-1 to J. B., PA 861/15-1 to R. P. The monoclonal antibody facility and the Chair of Vascular Biology are funded by the DFG under Germany's Excellence Strategy within the framework of the Munich Cluster for Systems Neurology (EXC 2145 SyNergy; ID 390857198). The Service Unit for Metabolomics and Lipidomics and the Department of Plant Biochemistry are supported by a grant of the DFG (INST 186/822-1) to I. F.

Conflict of interest—The authors declare that they have no conflicts of interest with the contents of this article.

Abbreviations—The abbreviations used are: ABA, abscisic acid; ANOVA, analysis of variance; AWF, apoplastic wash fluid; CLSM, confocal laser scanning microscopy; co-IP, co-immunoprecipitation; DAPI, 4′,6-diamidino-2-phenylindole; D-DT, D-dopachrome tautomerase; dpi, days post inoculation; hpi, hours post inoculation; ICA, indole-3-carboxylic acid; JA-Ile, jasmonic acid-isoleucine; LD, long-day; MDL, MIF/D-DT-like protein; MIF, macrophage migration inhibitory factor; NHP, *N*-hydroxy-pipecolic acid; OD_{600}, optical density at 600 nm; ORF, open reading frame; RLU, relative light units; RT-PCR, reverse transcription-polymerase chain reaction; SA, salicylic acid; SAR, systemic acquired resistance; SD, short-day; SDS-PAGE, sodium dodecylsulfate–polyacrylamide gel electrophoresis; Y2H, yeast two-hybrid.

References

1. Calandra, T., and Roger, T. (2003) Macrophage migration inhibitory factor: A regulator of innate immunity. *Nat. Rev. Immunol.* **3**, 791–800
2. David, J. R. (1966) Delayed hypersensitivity *in vitro*: Its mediation by cell-free substances formed by lymphoid cell-antigen interaction. *Proc. Natl. Acad. Sci. U. S. A.* **56**, 72–77
3. Kapurniotu, A., Gokce, O., and Bernhagen, J. (2019) The multitasking potential of alarmins and atypical chemokines. *Front. Med.* **6**, 3
4. Kang, I., and Bucala, R. (2019) The immunobiology of MIF: Function, genetics and prospects for precision medicine. *Nat. Rev. Rheumatol.* **15**, 427–437
5. Morand, E. F., Leech, M., and Bernhagen, J. (2006) Mif: A new cytokine link between rheumatoid arthritis and atherosclerosis. *Nat. Rev. Drug Discov.* **5**, 399–410
6. Sinitski, D., Kontos, C., Krammer, C., Asare, Y., Kapurniotu, A., and Bernhagen, J. (2019) Macrophage Migration Inhibitory Factor (MIF)-based therapeutic concepts in atherosclerosis and inflammation. *Thromb. Haemost.* **119**, 553–566
7. Tilstam, P. V., Qi, D., Leng, L., Young, L., and Bucala, R. (2017) MIF family cytokines in cardiovascular diseases and prospects for precision-based therapeutics. *Expert Opin. Ther. Targets* **21**, 671–683
8. Flieger, O., Engling, A., Bucala, R., Lue, H., Nickel, W., and Bernhagen, J. (2003) Regulated secretion of macrophage migration inhibitory factor is mediated by a non-classical pathway involving an ABC transporter. *FEBS Lett.* **551**, 78–86
9. Leng, L., Metz, C. N., Fang, Y., Xu, J., Donnelly, S., Baugh, J., Delohery, T., Chen, Y., Mitchell, R. A., and Bucala, R. (2003) MIF signal transduction initiated by binding to CD74. *J. Exp. Med.* **197**, 1467–1476
10. Bernhagen, J., Krohn, R., Lue, H., Gregory, J. L., Zernecke, A., Koenen, R. R., Dewor, M., Georgiev, I., Schober, A., Leng, L., Kooistra, T., Fingerle-Rowson, G., Ghezzi, P., Kleemann, R., McColl, S. R., *et al.* (2007) MIF is a noncognate ligand of CXC chemokine receptors in inflammatory and atherogenic cell recruitment. *Nat. Med.* **13**, 587–596
11. Borghese, F., and Clanchy, F. I. L. (2011) CD74: An emerging opportunity as a therapeutic target in cancer and autoimmune disease. *Expert Opin. Ther. Targets* **15**, 237–251
12. Rosengren, E., Bucala, R., Åman, P., Jacobsson, L., Odh, G., Metz, C. N., and Rorsman, H. (1996) The immunoregulatory mediator macrophage Migration Inhibitory Factor (MIF) catalyzes a tautomerization reaction. *Mol. Med.* **2**, 143–149
13. Kleemann, R., Kapurniotu, A., Frank, R. W., Gessner, A., Mischke, R., Flieger, O., Jüttner, S., Brunner, H., and Bernhagen, J. (1998) Disulfide analysis reveals a role for macrophage migration inhibitory factor (MIF) as thiol-protein oxidoreductase. *J. Mol. Biol.* **280**, 85–102
14. Wang, Y., An, R., Umanah, G. K., Park, H., Nambiar, K., Eacker, S. M., Kim, B., Bao, L., Harraz, M. M., Chang, C., Chen, R., Wang, J. E., Kam, T.-I., Jeong, J. S., Xie, Z., *et al.* (2016) A nuclease that mediates cell death induced by DNA damage and poly(ADP-ribose) polymerase-1. *Science* **354**, aad6872
15. Israelson, A., Ditsworth, D., Sun, S., Song, S., Liang, J., Hruska-Plochan, M., McAlonis-Downes, M., Abu-Hamad, S., Zoltsman, G., Shani, T., Maldonado, M., Bui, A., Navarro, M., Zhou, H., Marsala, M., *et al.* (2015) Macrophage migration inhibitory factor as a chaperone inhibiting accumulation of misfolded SOD1. *Neuron* **86**, 218–232
16. Merk, M., Mitchell, R. A., Endres, S., and Bucala, R. (2012) D-dopachrome tautomerase (D-DT or MIF-2): Doubling the MIF cytokine family. *Cytokine* **59**, 10–17
17. Merk, M., Zierow, S., Leng, L., Das, R., Du, X., Schulte, W., Fan, J., Lue, H., Chen, Y., Xiong, H., Chagnon, F., Bernhagen, J., Lolis, E., Mor, G., Lesur, O., *et al.* (2011) The *D*-dopachrome tautomerase (*DDT*) gene product is a cytokine and functional homolog of macrophage migration inhibitory factor (MIF). *Proc. Natl. Acad. Sci. U. S. A.* **108**, 85

18. Michelet, C., Danchin, E. G. J., Jaouannet, M., Bernhagen, J., Panstruga, R., Kogel, K.-H., Keller, H., and Coustau, C. (2019) Cross-kingdom analysis of diversity, evolutionary history, and site selection within the eukaryotic macrophage migration inhibitory factor superfamily. *Genes* **10**, E740
19. Sparkes, A., Baetselier, P. de, Roelants, K., Trez, C. de, Magez, S., van Ginderachter, J. A., Raes, G., Bucala, R., and Stijlemans, B. (2017) The non-mammalian MIF superfamily. *Immunobiology* **222**, 473–482
20. Panstruga, R., Baumgarten, K., and Bernhagen, J. (2015) Phylogeny and evolution of plant macrophage migration inhibitory factor/D-dopachrome tautomerase-like proteins. *BMC Evol. Biol.* **15**, 64
21. Sinitski, D., Gruner, K., Brandhofer, M., Kontos, C., Winkler, P., Reinstädler, A., Bourilhon, P., Xiao, Z., Cool, R., Kapurniotu, A., Dekker, F. J., Panstruga, R., and Bernhagen, J. (2020) Cross-kingdom mimicry of the receptor signaling and leukocyte recruitment activity of a human cytokine by its plant orthologs. *J. Biol. Chem.* **295**, 850–867
22. Foley, J. F. (2020) Plant chemokine mimics. *Sci. Signal.* **13**, eabb0387
23. Kamir, D., Zierow, S., Leng, L., Cho, Y., Diaz, Y., Griffith, J., McDonald, C., Merk, M., Mitchell, R. A., Trent, J., Chen, Y., Kwong, Y.-K. A., Xiong, H., Vermeire, J., Cappello, M., *et al.* (2008) A *Leishmania* ortholog of macrophage migration inhibitory factor modulates host macrophage responses. *J. Immunol.* **180**, 8250–8261
24. Naessens, E., Dubreuil, G., Giordanengo, P., Baron, O. L., Minet-Kebdani, N., Keller, H., and Coustau, C. (2015) A secreted MIF cytokine enables aphid feeding and represses plant immune responses. *Curr. Biol.* **25**, 1898–1903
25. Zybailov, B., Rutschow, H., Friso, G., Rudella, A., Emanuelsson, O., Sun, Q., van Wijk, and Klaas, J. (2008) Sorting signals, N-terminal modifications and abundance of the chloroplast proteome. *PLoS One* **3**, e1994
26. Olinares, Paul Dominic, B., Ponnala, L., van Wijk, and Klaas, J. (2010) Megadalton complexes in the chloroplast stroma of *Arabidopsis thaliana* characterized by size exclusion chromatography, mass spectrometry, and hierarchical clustering. *Mol. Cell. Proteomics* **9**, 1594–1615
27. Reumann, S., Babujee, L., Ma, C., Wienkoop, S., Siemsen, T., Antonicelli, G. E., Rasche, N., Lüder, F., Weckwerth, W., and Jahn, O. (2007) Proteome analysis of Arabidopsis leaf peroxisomes reveals novel targeting peptides, metabolic pathways, and defense mechanisms. *Plant Cell* **19**, 3170–3193
28. Pan, R., Reumann, S., Lisik, P., Tietz, S., Olsen, L. J., and Hu, J. (2018) Proteome analysis of peroxisomes from dark-treated senescent Arabidopsis leaves. *J. Integr. Plant Biol.* **60**, 1028–1050
29. Jedd, G., and Chua, N. H. (2002) Visualization of peroxisomes in living plant cells reveals acto-myosin-dependent cytoplasmic streaming and peroxisome budding. *Plant Cell Physiol.* **43**, 384–392
30. Weßling, R., Epple, P., Altmann, S., He, Y., Yang, L., Henz, S. R., McDonald, N., Wiley, K., Bader, K. C., Gläßer, C., Mukhtar, M. S., Haigis, S., Ghamsari, L., Stephens, A. E., Ecker, J. R., *et al.* (2014) Convergent targeting of a common host protein-network by pathogen effectors from three kingdoms of life. *Cell Host Microbe* **16**, 364–375
31. Arabidopsis Interactome Mapping Consortium (2011) Evidence for network evolution in an *Arabidopsis* interactome map. *Science* **333**, 601–607
32. Hartmann, U., Höhmann, S., Nettesheim, K., Wisman, E., Saedler, H., and Huijser, P. (2000) Molecular cloning of *SVP*: A negative regulator of the floral transition in *Arabidopsis*. *Plant J.* **21**, 351–360
33. Laubinger, S., Marchal, V., Le Gourrierec, J., Gentilhomme, J., Wenkel, S., Adrian, J., Jang, S., Kulajta, C., Braun, H., Coupland, G., and Hoecker, U. (2006) *Arabidopsis* SPA proteins regulate photoperiodic flowering and interact with the floral inducer CONSTANS to regulate its stability. *Development* **133**, 3213–3222
34. Kuhn, H., Kwaaitaal, M., Kusch, S., Acevedo-Garcia, J., Wu, H., and Panstruga, R. (2016) Biotrophy at its best: Novel findings and unsolved mysteries of the Arabidopsis-powdery mildew pathosystem. *The Arabidopsis Book* **14**, e0184
35. Consonni, C., Humphry, M. E., Hartmann, H. A., Livaja, M., Durner, J., Westphal, L., Vogel, J., Lipka, V., Kemmerling, B., Schulze-Lefert, P., Somerville, S. C., and Panstruga, R. (2006) Conserved requirement for a plant host cell protein in powdery mildew pathogenesis. *Nat. Genet.* **38**, 716–720
36. Acevedo-Garcia, J., Gruner, K., Reinstädler, A., Kemen, A., Kemen, E., Cao, L., Takken, F. L. W., Reitz, M. U., Schäfer, P., O'Connell, R. J., Kusch, S., Kuhn, H., and Panstruga, R. (2017) The powdery mildew-resistant Arabidopsis *mlo2 mlo6 mlo12* triple mutant displays altered infection phenotypes with diverse types of phytopathogens. *Sci. Rep.* **7**, 27
37. Lipka, V., Dittgen, J., Bednarek, P., Bhat, R., Wiermer, M., Stein, M., Landtag, J., Brandt, W., Rosahl, S., Scheel, D., Llorente, F., Molina, A., Parker, J., Somerville, S., and Schulze-Lefert, P. (2005) Pre- and post-invasion defenses both contribute to nonhost resistance in *Arabidopsis*. *Science* **310**, 1180–1183
38. Bednarek, P., Piślewska-Bednarek, M., Svatoš, A., Schneider, B., Doubský, J., Mansurova, M., Humphry, M., Consonni, C., Panstruga, R., Sanchez-Vallet, A., Molina, A., and Schulze-Lefert, P. (2009) A glucosinolate metabolism pathway in living plant cells mediates broad-spectrum antifungal defense. *Science* **323**, 101–106
39. Fan, J., Crooks, C., and Lamb, C. (2008) High-throughput quantitative luminescence assay of the growth *in planta* of *Pseudomonas syringae* chromosomally tagged with *Photorhabdus luminescens luxCDABE*. *Plant J.* **53**, 393–399
40. Gruner, K., Zeier, T., Aretz, C., and Zeier, J. (2018) A critical role for Arabidopsis MILDEW RESISTANCE LOCUS O2 in systemic acquired resistance. *Plant J.* **94**, 1064–1082
41. Durrant, W. E., and Dong, X. (2004) Systemic acquired resistance. *Annu. Rev. Phytopathol.* **42**, 185–209
42. Bernsdorff, F., Döring, A.-C., Gruner, K., Schuck, S., Bräutigam, A., and Zeier, J. (2016) Pipecolic acid orchestrates plant systemic acquired resistance and defense priming via salicylic acid-dependent and -independent pathways. *Plant Cell* **28**, 102–129
43. Hartmann, M., Zeier, T., Bernsdorff, F., Reichel-Deland, V., Kim, D., Hohmann, M., Scholten, N., Schuck, S., Bräutigam, A., Hölzel, T., Ganter, C., and Zeier, J. (2018) Flavin monooxygenase-generated N-hydroxypipecolic acid is a critical element of plant systemic immunity. *Cell* **173**, 456–469.e16
44. Mishina, T. E., and Zeier, J. (2007) Pathogen-associated molecular pattern recognition rather than development of tissue necrosis contributes to bacterial induction of systemic acquired resistance in Arabidopsis. *Plant J.* **50**, 500–513
45. Ding, P., and Ding, Y. (2020) Stories of salicylic acid: A plant defense hormone. *Trends Plant Sci.* **25**, 549–565
46. Nawrath, C., and Metraux, J. P. (1999) Salicylic acid induction-deficient mutants of Arabidopsis express *PR-2* and *PR-5* and accumulate high levels of camalexin after pathogen inoculation. *Plant Cell* **11**, 1393–1404
47. Wildermuth, M. C., Dewdney, J., Wu, G., and Ausubel, F. M. (2001) Isochorismate synthase is required to synthesize salicylic acid for plant defence. *Nature* **414**, 562–565
48. Holowka, T., and Bucala, R. (2020) Role of host and parasite MIF cytokines during *Leishmania* infection. *Trop. Med. Infect. Dis.* **5**, 46
49. Sun, T., Holowka, T., Song, Y., Zierow, S., Leng, L., Chen, Y., Xiong, H., Griffith, J., Nouraie, M., Thuma, P. E., Lolis, E., Janse, C. J., Gordeuk, V. R., Augustijn, K., and Bucala, R. (2012) A Plasmodium-encoded cytokine suppresses T-cell immunity during malaria. *Proc. Natl. Acad. Sci. U. S. A.* **109**, E2117–E2126
50. Holowka, T., Castilho, T. M., Garcia, A. B., Sun, T., McMahon-Pratt, D., and Bucala, R. (2016) *Leishmania*-encoded orthologs of macrophage migration inhibitory factor regulate host immunity to promote parasite persistence. *FASEB J.* **30**, 2249–2265
51. Baeza Garcia, A., Siu, E., Sun, T., Exler, V., Brito, L., Hekele, A., Otten, G., Augustijn, K., Janse, C. J., Ulmer, J. B., Bernhagen, J., Fikrig, E., Geall, A., and Bucala, R. (2018) Neutralization of the *Plasmodium*-encoded MIF ortholog confers protective immunity against malaria infection. *Nat. Commun.* **9**, 2714
52. Sinitski, D., Gruner, K., Bernhagen, J., and Panstruga, R. (2020) Studying plant MIF/D-DT-like genes and proteins (MDLs). *Methods Mol. Biol.* **2080**, 249–261
53. Niehaus, T. D., Thamm, A. M. K., Crécy-Lagard, V. de, and Hanson, A. D. (2015) Proteins of unknown biochemical function: A persistent problem and a roadmap to help overcome it. *Plant Physiol.* **169**, 1436–1442
54. Li, J.-F., Park, E., von Arnim, Albrecht, G., and Nebenführ, A. (2009) The FAST technique: A simplified *Agrobacterium*-based transformation

method for transient gene expression analysis in seedlings of Arabidopsis and other plant species. *Plant Methods* **5**, 6
55. Sun, H. W., Bernhagen, J., Bucala, R., and Lolis, E. (1996) Crystal structure at 2.6-Å resolution of human macrophage migration inhibitory factor. *Proc. Natl. Acad. Sci. U. S. A.* **93**, 5191–5196
56. Fan, C., Rajasekaran, D., Syed, M. A., Leng, L., Loria, J. P., Bhandari, V., Bucala, R., and Lolis, E. J. (2013) MIF intersubunit disulfide mutant antagonist supports activation of CD74 by endogenous MIF trimer at physiologic concentrations. *Proc. Natl. Acad. Sci. U. S. A.* **110**, 10994–10999
57. Philo, J. S., Yang, T.-H., and LaBarre, M. (2004) Re-examining the oligomerization state of macrophage migration inhibitory factor (MIF) in solution. *Biophys. Chem.* **108**, 77–87
58. Andrés, F., and Coupland, G. (2012) The genetic basis of flowering responses to seasonal cues. *Nat. Rev. Genet.* **13**, 627–639
59. van Wersch, R., Li, X., and Zhang, Y. (2016) Mighty dwarfs: *Arabidopsis* autoimmune mutants and their usages in genetic dissection of plant immunity. *Front. Plant Sci.* **7**, 1717
60. Ellis, C., Karafyllidis, L., and Turner, J. G. (2002) Constitutive activation of jasmonate signaling in an *Arabidopsis* mutant correlates with enhanced resistance to *Erysiphe cichoracearum*, *Pseudomonas syringae*, and *Myzus persicae*. *Mol. Plant-Microbe Interact.* **15**, 1025–1030
61. Bowling, S. A., Guo, A., Cao, H., Gordon, A. S., Klessig, D. F., and Dong, X. (1994) A mutation in Arabidopsis that leads to constitutive expression of systemic acquired resistance. *Plant Cell* **6**, 1845–1857
62. Bowling, S. A., Clarke, J. D., Liu, Y., Klessig, D. F., and Dong, X. (1997) The *cpr5* mutant of Arabidopsis expresses both NPR1-dependent and NPR1-independent resistance. *Plant Cell* **9**, 1573–1584
63. He, Q., Naqvi, S., McLellan, H., Boevink, P. C., Champouret, N., Hein, I., and Birch, P. R. J. (2018) Plant pathogen effector utilizes host susceptibility factor NRL1 to degrade the immune regulator SWAP70. *Proc. Natl. Acad. Sci. U. S. A.* **115**, E7834–E7843
64. Turnbull, D., Wang, H., Breen, S., Malec, M., Naqvi, S., Yang, L., Welsh, L., Hemsley, P., Zhendong, T., Brunner, F., Gilroy, E. M., and Birch, P. R. J. (2019) AVR2 targets BSL family members, which act as susceptibility factors to suppress host immunity. *Plant Physiol.* **180**, 571–581
65. Li, H., Wang, H., Jing, M., Zhu, J., Guo, B., Wang, Y., Lin, Y., Chen, H., Kong, L., Ma, Z., Wang, Y., Ye, W., Dong, S., Tyler, B., and Wang, Y. (2018) A *Phytophthora* effector recruits a host cytoplasmic transacetylase into nuclear speckles to enhance plant susceptibility. *eLife* **7**, e40039
66. Park, C.-H., Chen, S., Shirsekar, G., Zhou, B., Khang, C. H., Songkumarn, P., Afzal, A. J., Ning, Y., Wang, R., Bellizzi, M., Valent, B., and Wang, G.-L. (2012) The *Magnaporthe oryzae* effector AvrPiz-t targets the RING E3 ubiquitin ligase APIP6 to suppress pathogen-associated molecular pattern-triggered immunity in rice. *Plant Cell* **24**, 4748–4762
67. Pavan, S., Jacobsen, E., Visser, R. G. F., and Bai, Y. (2010) Loss of susceptibility as a novel breeding strategy for durable and broad-spectrum resistance. *Mol. Breed.* **25**, 1–12
68. Tynan, A., Mawhinney, L., Armstrong, M. E., O'Reilly, C., Kennedy, S., Caraher, E., Jülicher, K., O'Dwyer, D., Maher, L., Schaffer, K., Fabre, A., McKone, E. F., Leng, L., Bucala, R., Bernhagen, J., *et al.* (2017) Macrophage migration inhibitory factor enhances *Pseudomonas aeruginosa* biofilm formation, potentially contributing to cystic fibrosis pathogenesis. *FASEB J.* **31**, 5102–5110
69. Shao, X., Xie, Y., Zhang, Y., and Deng, X. (2019) Biofilm formation assay in *Pseudomonas syringae*. *Bio Protoc.* **9**, e3237
70. Assaad, F. F., Qiu, J. L., Youngs, H., Ehrhardt, D., Zimmerli, L., Kalde, M., Wanner, G., Peck, S. C., Edwards, H., Ramonell, K., Somerville, C. R., and Thordal-Christensen, H. (2004) The PEN1 syntaxin defines a novel cellular compartment upon fungal attack and is required for the timely assembly of papillae. *Mol. Biol. Cell* **15**, 5118–5129
71. Bhat, R. A., Miklis, M., Schmelzer, E., Schulze-Lefert, P., and Panstruga, R. (2005) Recruitment and interaction dynamics of plant penetration resistance components in a plasma membrane microdomain. *Proc. Natl. Acad. Sci. U. S. A.* **102**, 3135–3140
72. Underwood, W., and Somerville, S. C. (2013) Perception of conserved pathogen elicitors at the plasma membrane leads to relocalization of the Arabidopsis PEN3 transporter. *Proc. Natl. Acad. Sci. U. S. A.* **110**, 12492–12497
73. Underwood, W., Ryan, A., and Somerville, S. C. (2017) An *Arabidopsis* lipid flippase is required for timely recruitment of defenses to the host-pathogen interface at the plant cell surface. *Mol. Plant* **10**, 805–820
74. Lyons, R., Rusu, A., Stiller, J., Powell, J., Manners, J. M., and Kazan, K. (2015) Investigating the association between flowering time and defense in the *Arabidopsis thaliana-Fusarium oxysporum* interaction. *PLoS One* **10**, e0127699
75. Lai, Z., Schluttenhofer, C. M., Bhide, K., Shreve, J., Thimmapuram, J., Lee, S. Y., Yun, D.-J., and Mengiste, T. (2014) MED18 interaction with distinct transcription factors regulates multiple plant functions. *Nat. Commun.* **5**, 3064
76. Martínez, C., Pons, E., Prats, G., and León, J. (2004) Salicylic acid regulates flowering time and links defence responses and reproductive development. *Plant J.* **37**, 209–217
77. Song, S., Qi, T., Fan, M., Zhang, X., Gao, H., Huang, H., Wu, D., Guo, H., and Xie, D. (2013) The bHLH subgroup IIId factors negatively regulate jasmonate-mediated plant defense and development. *PLoS Genet.* **9**, e1003653
78. Ogawara, T., Higashi, K., Kamada, H., and Ezura, H. (2003) Ethylene advances the transition from vegetative growth to flowering in *Arabidopsis thaliana*. *J. Plant Physiol.* **160**, 1335–1340
79. Alonso, J. M., Stepanova, A. N., Leisse, T. J., Kim, C. J., Chen, H. M., Shinn, P., Stevenson, D. K., Zimmerman, J., Barajas, P., Cheuk, R., Gadrinab, C., Heller, C., Jeske, A., Koesema, E., Meyers, C. C., *et al.* (2003) Genome-wide insertional mutagenesis of *Arabidopsis thaliana*. *Science* **301**, 653–657
80. Li, W., Yadeta, K. A., Elmore, J. M., and Coaker, G. (2013) The *Pseudomonas syringae* effector HopQ1 promotes bacterial virulence and interacts with tomato 14-3-3 proteins in a phosphorylation-dependent manner. *Plant Physiol.* **161**, 2062–2074
81. Czechowski, T., Stitt, M., Altmann, T., Udvardi, M. K., and Scheible, W. R. (2005) Genome-wide identification and testing of superior reference genes for transcript normalization in Arabidopsis. *Plant Physiol.* **139**, 5–17
82. Wu, F.-H., Shen, S.-C., Lee, L.-Y., Lee, S.-H., Chan, M.-T., and Lin, C.-S. (2009) Tape-*Arabidopsis* Sandwich - a simpler Arabidopsis protoplast isolation method. *Plant Methods* **5**, 16
83. Clough, S. J., and Bent, A. F. (1998) Floral dip: A simplified method for *Agrobacterium*-mediated transformation of *Arabidopsis thaliana*. *Plant J.* **16**, 735–743
84. Bartsch, M., Gobbato, E., Bednarek, P., Debey, S., Schultze, J. L., Bautor, J., and Parker, J. E. (2006) Salicylic acid-independent ENHANCED DISEASE SUSCEPTIBILITY1 signaling in *Arabidopsis* immunity and cell death is regulated by the monooxygenase *FMO1* and the nudix hydrolase *NUDT7*. *Plant Cell* **18**, 1038–1051
85. Campe, R., Langenbach, C., Leissing, F., Popescu, G. V., Popescu, S. C., Goellner, K., Beckers, Gerold J. M., and Conrath, U. (2016) ABC transporter PEN3/PDR8/ABCG36 interacts with calmodulin that, like PEN3, is required for Arabidopsis nonhost resistance. *New Phytol.* **209**, 294–306
86. Bradford, M. M. (1976) A rapid and sensitive method for the quantitation of microgram quantities of protein utilizing the principle of protein-dye binding. *Anal. Biochem.* **72**, 248–254
87. Feederle, R., Gerber, J.-K., Middleton, A., Northrup, E., Kist, R., Kremmer, E., and Peters, H. (2016) Generation of Pax1/PAX1-specific monoclonal antibodies. *Monoclon. Antib. Immunodiagn. Immunother.* **35**, 259–262
88. Köhler, G., and Milstein, C. (1975) Continuous cultures of fused cells secreting antibody of predefined specificity. *Nature* **256**, 495–497
89. Altmann, M., Altmann, S., Falter, C., and Falter-Braun, P. (2018) High-quality yeast-2-hybrid interaction network mapping. *Curr. Protoc. Plant Biol.* **3**, e20067
90. Herrfurth, C., and Feussner, I. (2020) Quantitative jasmonate profiling using a high-throughput UPLC-nanoESI-MS/MS method. *Methods Mol. Biol.* **2085**, 169–187
91. Mohnike, L., Rekhter, D., Huang, W., Feussner, K., Tian, H., Herrfurth, C., Zhang, Y., and Feussner, I. (2021) The glycosyltransferase UGT76B1 modulates *N*-hydroxy-pipecolic acid homoeostasis and plant immunity. *Plant Cell*